

(200)
T67r
no. 597

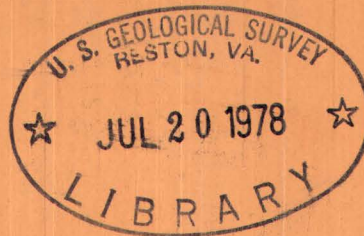
Unclassified

Coleman

Mineralogical applications of electron diffraction.

1. Theory and techniques

By Malcolm Ross and C. L. Christ



Trace Elements Investigations Report 597

UNITED STATES DEPARTMENT OF THE INTERIOR
GEOLOGICAL SURVEY

Geology and Mineralogy

UNITED STATES DEPARTMENT OF THE INTERIOR
GEOLOGICAL SURVEY

MINERALOGICAL APPLICATIONS OF ELECTRON DIFFRACTION.

I. THEORY AND TECHNIQUES*

By

Malcolm Ross and C. L. Christ

March 1958

Trace Elements Investigations Report 597

This preliminary report is distributed without editorial and technical review for conformity with official standards and nomenclature. It is not for public inspection or quotation.

*This report concerns work done on behalf of the Division of Research of the U. S. Atomic Energy Commission.

USGS - TEI-597

GEOLOGY AND MINERALOGY

<u>Distribution</u>	<u>No. of copies</u>
Division of Raw Materials, Albuquerque.....	1
Division of Raw Materials, Austin.....	1
Division of Raw Materials, Casper.....	1
Division of Raw Materials, Denver.....	1
Division of Raw Materials, Salt Lake City.....	1
Division of Raw Materials, Spokane.....	1
Division of Raw Materials, Washington	3
Division of Research, Washington	1
Grand Junction Operations Office	1
Production Evaluation Division, GJOO.....	1
Technical Information Service Extension, Oak Ridge.....	6
U.S. Geological Survey:	
Foreign Geology Branch, Washington	1
Fuels Branch, Washington	1
Geochemistry and Petrology Branch, Washington	12
Geophysics Branch, Washington	1
Mineral Deposits Branch, Washington	1
P. E. Hotz, Menlo Park	1
E. M. MacKevett, Menlo Park	1
L. R. Page, Washington	1
P. K. Sims, Denver	1
Q. D. Singewald, Beltsville	1
A. E. Weissenborn, Spokane	1
TEPCO, Denver	2
TEPCO, RPS, Washington, (including master).....	2

CONTENTS

	Page
Abstract	6
Introduction	7
Theory of interpretation of single-crystal patterns	8
Description of instruments	10
Sample preparation and examination	12
Standardization of electron-diffraction patterns	14
Analysis of single-crystal patterns of colemanite	16
Interpretation of patterns	16
Measurement of patterns	23
Analysis of single-crystal patterns of $KClO_3$	34
Interpretation of patterns	34
Measurement of patterns	39
Discussion	47
References	54

ILLUSTRATIONS

Figure 1. The experimental arrangement for obtaining transmission electron-diffraction patterns	9
2. The Ewald construction for the diffraction of electrons showing the reciprocal lattice points extended into rods	11
3a. EDU spot pattern of colemanite	17
3b. Indexed reproduction of the EDU spot pattern of colemanite shown in figure 3a	18

	Page
Figure 4a. EDU spot pattern of colemanite	19
4b. Indexed reproduction of the EDU spot pattern of colemanite shown in figure 4a	20
5. Ewald construction showing a portion of the section of the colemanite reciprocal lattice through the origin and perpendicular to the <u>c</u> -axis ($\lambda = 0.0534$ A).21	21
6a. SAD spot pattern of colemanite superimposed upon the powder pattern of the internal aluminum standard	24
6b. Indexed reproduction of the SAD spot pattern of colemanite shown in figure 6a	25
7. Electron micrograph of the colemanite crystal from which SAD spot pattern shown in figure 6a was made..	26
8. The Ewald construction used to evaluate the error in reciprocal lattice spacings given by electron diffraction patterns	27
9. Graph for evaluating the factor $(\cos 2\theta_g)/(\cos 2\theta \cos \theta_g)$ for a given direct lattice spacing	33
10. The position of the specimen mount and the $KClO_3$ crystal in relation to the electron beam.....	35
11a. EDU spot pattern of $KClO_3$ ($h0\bar{l}$) superimposed upon the powder pattern of the internal β -tin standard	36
11b. Indexed reproduction of the EDU spot pattern of $KClO_3$ shown in figure 11a	37
12. Ewald construction showing a portion of the section of the $KClO_3$ reciprocal lattice through the origin and perpendicular to the <u>b</u> -axis ($\lambda = 0.0534$ A)	38
13a. EDU spot pattern of $KClO_3$ ($0k\bar{l}$) superimposed upon the powder pattern of the internal β -tin standard	40
13b. Indexed reproduction of the EDU spot pattern of $KClO_3$ shown in figure 13a	41
14. Ewald construction showing a portion of the section of the $KClO_3$ reciprocal lattice through the origin and perpendicular to the <u>a</u> -axis ($\lambda = 0.0534$ A)	42

	Page
Figure 15. Geometrical construction used to evaluate the projection of the (hk0) reciprocal net of KClO_3 onto the <u>a-b</u> plane	43
16a. EDU pattern taken after a single crystal of KClO_3 had been centered in the electron beam for ten minutes	48
16b. Indexed reproduction of the EDU pattern shown in figure 16a	49

TABLES

Table 1. Single crystal data: Colemanite, $\text{CaB}_3\text{O}_4(\text{OH})_3 \cdot \text{H}_2\text{O}$, monoclinic	31
2. Values of the <u>a</u> and <u>b</u> unit-cell constants obtained from measurement of the higher order reflections of eight KClO_3 EDU single-crystal patterns	45
3. Single-crystal data: KClO_3 , monoclinic	46
4. Crystallographic data obtained directly from spot patterns of crystals belonging to the six crystal systems	51

MINERALOGICAL APPLICATIONS OF ELECTRON DIFFRACTION.

I. Theory and techniques

By Malcolm Ross and C. L. Christ

ABSTRACT

The small wavelengths used in electron-diffraction experiments and the thinness of the crystals necessary for the transmission of the electron beam combine to require a somewhat different diffraction geometry for the interpretation of electron-diffraction patterns than is used in the interpretation of X-ray diffraction patterns. This geometry, based on the reciprocal lattice concept and geometrical construction of Ewald, needed for the interpretation of transmission electron-diffraction single-crystal patterns is here reviewed.

Transmission electron-diffraction single-crystal patterns of two monoclinic substances, colemanite [$\text{CaB}_3\text{O}_4(\text{OH})_3 \cdot \text{H}_2\text{O}$] and potassium chlorate (KClO_3), are examined and the theory necessary for their interpretation is given in detail. The study of these patterns furnishes a basis for the interpretation of single-crystal patterns of materials belonging to any crystal system. It is shown that useful unit-cell data, accurate to a few tenths of a percent, can be obtained from the patterns of colemanite and KClO_3 . A method of evaluating unit-cell data from measurements of such single-crystal patterns is given.

The transmission electron-diffraction powder pattern obtained from an oriented aggregate of thin crystals gives the same unit-cell data as are given by the electron-diffraction single-crystal pattern obtained from one crystal of the aggregate. A graphical method is given for precisely evaluating unit-cell constants from measurements of such a powder pattern.

INTRODUCTION

Mineralogical applications of electron-diffraction techniques have been somewhat limited, partly because not all minerals are amenable to study by this method, and partly because of the extensive use of the X-ray diffraction method. Of particular interest to the mineralogist is the fact that symmetry-true, indexable single-crystal diffraction patterns can be obtained with electrons from very minute crystals contained within a sample which will give only a Debye-Scherrer pattern with X-rays. Because very small, individual crystals can be studied in this way, a given sample can be analyzed very thoroughly for crystalline components present in minor amounts, in contrast to the X-ray method which is relatively insensitive in this regard.

During the past few years, we have gained much experience in the application of the combined techniques of electron diffraction and electron microscopy to the study of mineralogical problems. This paper gives a description of the techniques developed, and the results obtained from a number of mineralogical studies. Part I of the paper contains a discussion of the experimental methods used in the work and a description of the theory used in the interpretation of single-crystal electron-diffraction patterns. The methods of interpreting and measuring single-crystal patterns of the monoclinic substances colemanite, $\text{CaB}_3\text{O}_4(\text{OH})_3 \cdot \text{H}_2\text{O}$, and potassium chlorate, KClO_3 , are treated in detail. Part II of the paper (Ross, 1958) gives partial unit-cell data for a number of fine-grained vanadium minerals.

This work is part of a program being conducted by the U. S. Geological Survey on behalf of the Division of Research of the U. S. Atomic Energy Commission.

THEORY OF INTERPRETATION OF SINGLE-CRYSTAL PATTERNS

In the present study, only transmission electron-diffraction patterns are considered. The experimental arrangement for obtaining such patterns is shown schematically in figure 1. If only one crystal lies in the path of the beam, a spot pattern is obtained; whereas if a large number of crystals lie in the path of the beam, a powder pattern is obtained. The powder pattern will show a number of continuous rings and is similar to the X-ray Debye-Scherrer pattern.

The most powerful method for the interpretation of single-crystal patterns is based on the reciprocal lattice concept. The reciprocal lattice is treated at length in James (1954). In the present paper his notation is followed with the exception that \underline{H} (present paper) = \underline{r}^* (James). It is useful to recall here the differences in the interference geometry for the diffraction of electrons and the diffraction of X-rays. The Ewald sphere has a radius of the order of 1 \AA^{-1} for the wavelengths ordinarily used in X-ray diffraction. In electron-diffraction experiments much smaller wavelengths are used. For example, for electrons accelerated under a potential of 50 kv, $\lambda = 0.0534 \text{ \AA}$. Corresponding to this case the Ewald sphere has a radius of 18.7 \AA^{-1} , and its surface approximates a plane relative to the reciprocal lattice. The nodes of the reciprocal lattice have the properties of mathematical points only for crystals that are ideally triperiodic. In the real crystal these nodes must be replaced by appropriate small volumes (rods, parallelepipeds, etc.) whose size and shape reflect the size and shape of the periodic continuum. For the case of interest in this paper, i.e., the very thin crystal, the

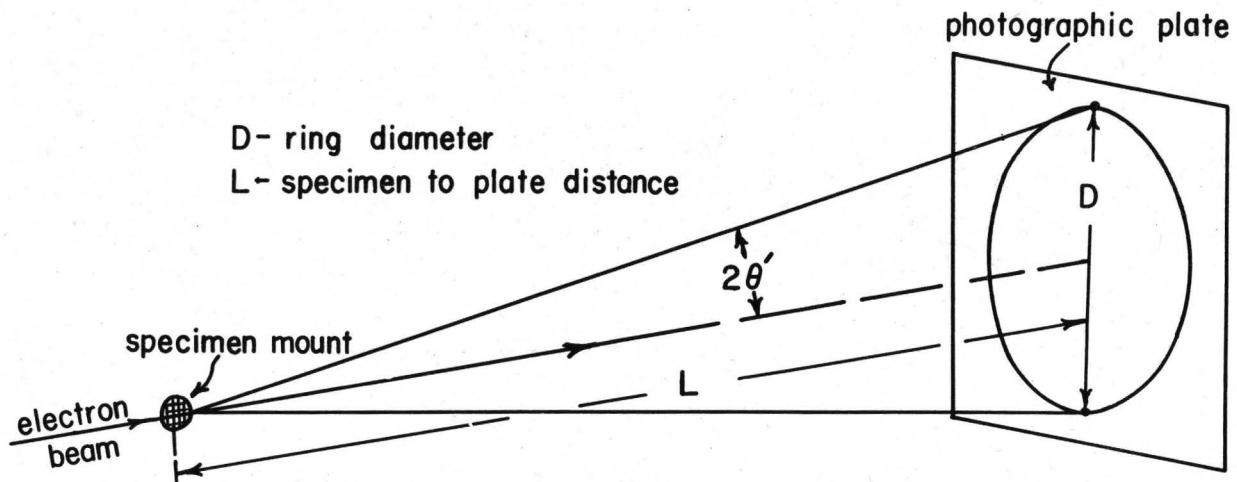


Figure 1.--The experimental arrangement for obtaining transmission electron-diffraction patterns.

reciprocal lattice points are replaced by rods having their lengths parallel to the thin direction of the crystal, with the total length p of each rod given by the relationship $p = 2/t$, where t is the thickness of the crystal. It can be seen from figure 2 that when the direction of the incident beam of electrons is parallel to the long direction of the reciprocal lattice rods (parallel to the thin direction of the crystal) the chances are greatly increased that some portion of the rod will intersect the Ewald sphere with ensuing diffraction. It can also be seen from figure 2 that the smaller the spacing of the reciprocal lattice in the thin direction of the crystal the greater are the chances that reciprocal lattice rods in the upper levels of the reciprocal lattice will intersect the sphere.

There are other factors that increase the possibility of meeting the interference condition. Lack of exact homogeneity in the wavelength of the electrons results in the transformation of the Ewald surface into a thin slab having a thickness determined by the spread in wavelengths. Variations in the direction of the incident beam and distortion in the lattice planes normal to the beam will also contribute to an increase in the number of diffraction spots observed.

DESCRIPTION OF INSTRUMENTS

The electron microscope used in this study (RCA, type EMU2B, 50 kv) is designed for study of particles in the range of 0.001 to 10 microns. This instrument is equipped with a selected area diffraction attachment which can be used to obtain diffraction patterns from specific areas of the sample. Hall (1953) gives a complete description of the electron microscope and Picard and

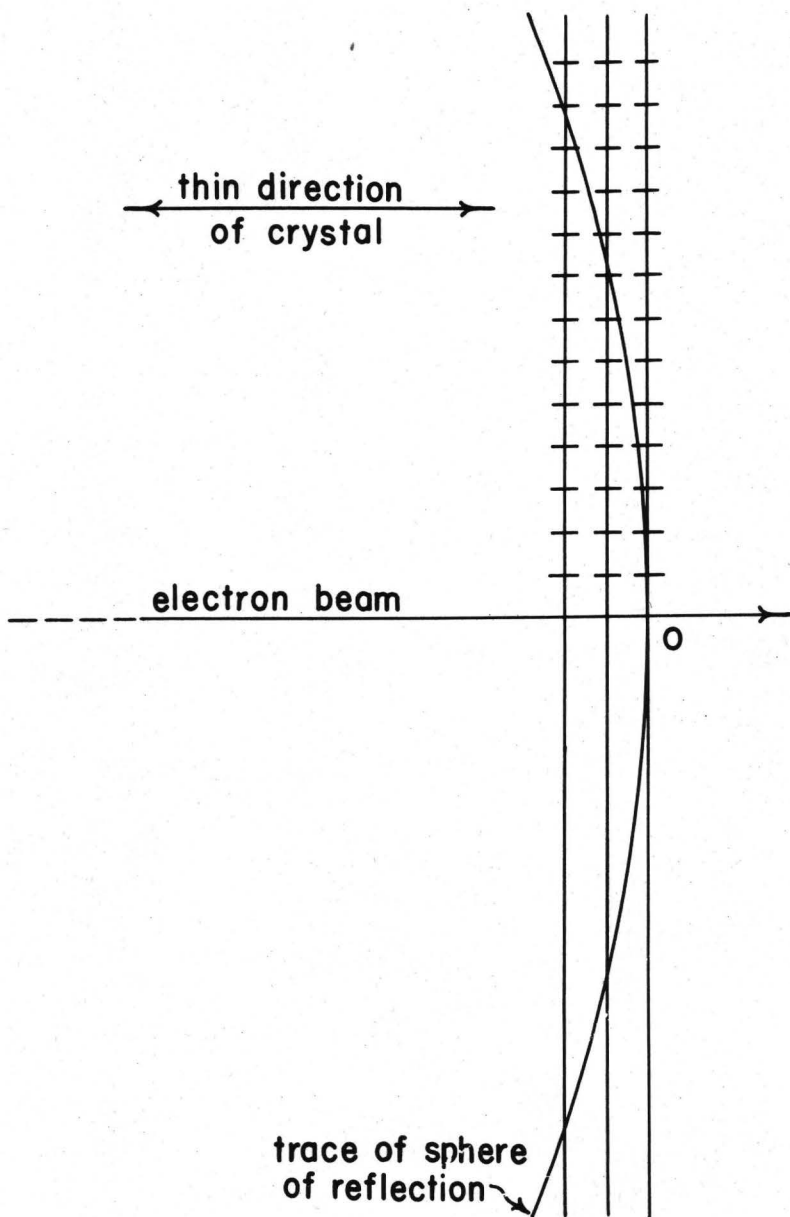


Figure 2.--The Ewald construction for the diffraction of electrons showing the reciprocal lattice points extended into rods.

Reisner (1946) discuss the use of the electron microscope as a diffraction camera.

A separate diffraction unit (RCA, type EMD) was used to obtain many of the patterns for this study. The unit is specifically designed for work with powder and single-crystal mounts using either reflection or transmission methods. The diffraction patterns are recorded on a 4 x 5 inch photographic plate and yield more precise measurements than the smaller patterns obtained with the electron microscope. A disadvantage of the electron-diffraction unit is that the crystals from which the diffraction patterns are obtained cannot be seen as they can be with the electron microscope. The diffraction unit is operated at a potential of 50 kv, d-c; the direct current is regulated to 1 part in 50,000 with a ripple of less than 2 volts peak-to-peak. The upper pole piece aperture has a diameter of 1/1000 inch. The specimen-to-plate distance for most of the patterns taken with this instrument is approximately 50 cm.

SAMPLE PREPARATION AND EXAMINATION

Samples are usually prepared by dispersing or dissolving the experimental material in distilled water. A droplet of the liquid is then placed on a 200-mesh stainless steel screen which has been previously covered by a collodion film, 50 to 150 Å thick. When an internal standard is desired aluminum or β-tin is vaporized in vacuum onto the collodion film prior to mounting the sample. A description of sample preparation techniques useful for this type of work was edited by Drumond (1950).

A preliminary examination of most samples is made with the electron microscope. The samples are checked for particle size, purity, orientation, and crystallinity. In general, single-crystal diffraction patterns ("spot" patterns) are obtained from individual crystals within the sample by converting the microscope into a diffraction camera. Usually an electron micrograph is made of the crystal or crystals producing the pattern. An example of this selected area diffraction technique, referred to as "SAD" in the following, can be seen in figure 6a.

After examination with the microscope the specimen mounts are transferred to the electron-diffraction unit and placed so that the collodion film is approximately normal to the electron beam. The mount is then traversed in a horizontal plane until a suitable spot or powder pattern is obtained. For spot patterns, adjustments in tilt of the specimen are made so that the intensities of spots related by a center of symmetry appear to be equal.

A second method of examining crystals with the electron-diffraction unit is sometimes used. A cleavage fragment, which must be thin enough in some areas to permit the transmission of the weakly penetrating electrons, is mounted on a holder that allows considerable freedom in the adjustment of the sample plane. The fragment is oriented so that the cleavage plane is approximately normal to the electron beam, and final adjustment is then made so that the resulting spot pattern appears symmetrical and spots related by a center of symmetry have approximately equal intensities. Hereafter we shall refer to patterns taken with the electron-diffraction unit as "EDU" patterns. In Part I all values given for unit-cell constants are obtained from measurements of EDU patterns.

STANDARDIZATION OF ELECTRON-DIFFRACTION PATTERNS

Evaluation of direct lattice spacings from EDU spot or powder patterns may be accomplished with fair accuracy provided the specimen-to-photographic plate distance and wavelength of the electrons are known. Referring to figure 1 we see that

$$\tan 2\theta' = \frac{D}{2L}$$

or

$$\frac{2 \sin \theta' \cos \theta'}{\cos 2\theta'} = \frac{D}{2L} \quad (1)$$

where D is the ring diameter (or the distance between spots related by a center of symmetry), L is the specimen-to-plate distance and θ' is the Bragg angle for the electron diffraction case. For small angles ^{1/}

$$\frac{\cos \theta'}{\cos 2\theta'} \cong 1. \quad (2)$$

On combining (1) and (2) we then have

$$\sin \theta' = \frac{D}{4L} \quad (3)$$

Substituting (3) into Bragg's law gives

$$\underline{d}' = \frac{2L\lambda}{D} \quad (4)$$

where \underline{d}' is the direct lattice spacing given by the diffraction pattern.

^{1/} Using 50 kv radiation ($\lambda = 0.0534$ A) $\cos \theta'$ never reaches a value smaller than 0.993 for \underline{d} -spacings greater than 0.7 A.

Since it is inconvenient to measure λ and L with high accuracy, another method is used in this laboratory to evaluate direct lattice spacings. This is done by comparing the electron-diffraction pattern of a standard material to that of the experimental material. This "standardization" of diffraction patterns can be accomplished in two ways. Collodion mounts previously coated with a thin layer of aluminum or β -tin are used for some specimen mounts. These yield photographs that show the diffraction pattern of the experimental material superimposed on the powder pattern of the standard substance. An example of this type of pattern may be seen in figure 11a. The second method of standardizing a pattern is to photograph the diffraction pattern of the experimental material and then immediately to photograph a pattern of the standard substance on another plate. This is done by traversing the specimen stage horizontally to bring a screen containing the standard directly under the beam. This operation involves no change in specimen-to-plate distance. The wavelength is assumed to be constant over the brief period required to make the two photographs.

As will be shown later, the direct lattice spacings of the standard and experimental materials are very nearly inversely proportional to the ring diameters provided that the standard and experimental materials are photographed at constant wavelength and specimen-to-plate distance, that is,

$$\frac{d_x}{d_s} \cong \frac{D_s}{D_x} \quad (5)$$

where d_x and d_s refer to the direct lattice spacings of the experimental and standard materials, respectively, and D_x and D_s refer to the ring diameters. Knowing d_s it is only necessary to measure D_x and D_s by some suitable means in order to calculate d_x .

Measurement of the spot or powder patterns is usually done with a measuring microscope. Another method of measurement found to be quite useful in evaluating parameters from single-crystal patterns is accomplished by enlarging the patterns of the standard and experimental materials photographically to about 5 times the original size and measuring the enlargements with a millimeter scale. This method has been found to give lattice parameters almost as precise as those evaluated from measurements obtained with a measuring microscope. Due to the appearance of a slight ellipticity in the diffraction patterns, care is taken to measure both the standard and experimental patterns over the same diameter.

ANALYSIS OF SINGLE-CRYSTAL PATTERNS OF COLEMANITE

Interpretation of patterns

Colemanite, $\text{CaB}_3\text{O}_4(\text{OH})_3 \cdot \text{H}_2\text{O}$, is monoclinic and has perfect cleavage parallel to (010). Single-crystal patterns of this mineral were obtained with the electron diffraction unit by mounting a thin cleavage fragment so that the cleavage plane was approximately normal to the electron beam. Figure 3a and 4a show spot patterns of colemanite obtained in this manner; the patterns are indexed as shown in figures 3b and 4b.

One method of interpreting these spot patterns, as previously discussed, is based on the reciprocal lattice concept. In figure 5, a portion of the section of the colemanite reciprocal lattice through the origin and perpendicular to the c-axis, is represented. It can be seen that the trace

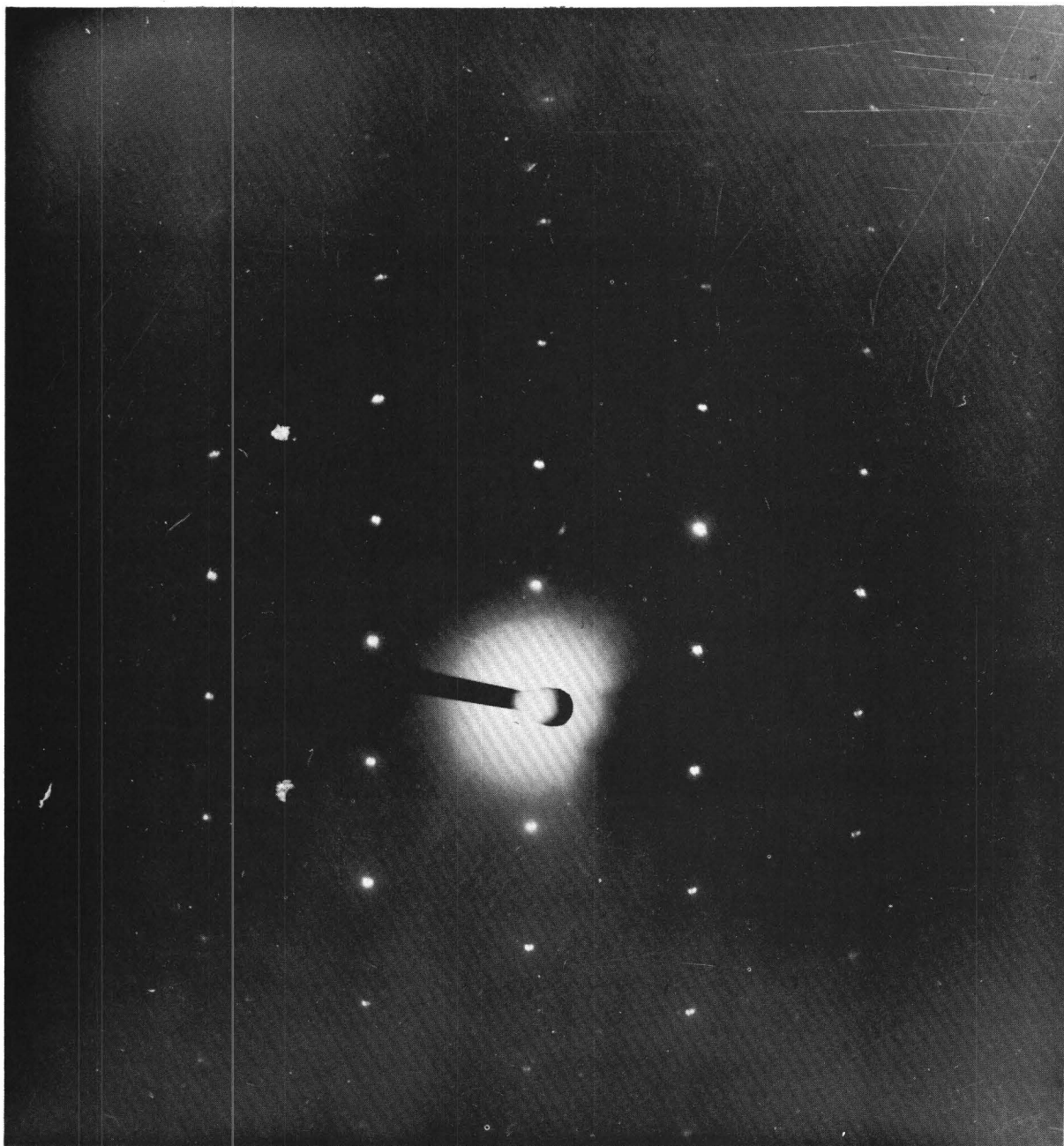


Figure 3a.--EDU spot pattern of colemanite.

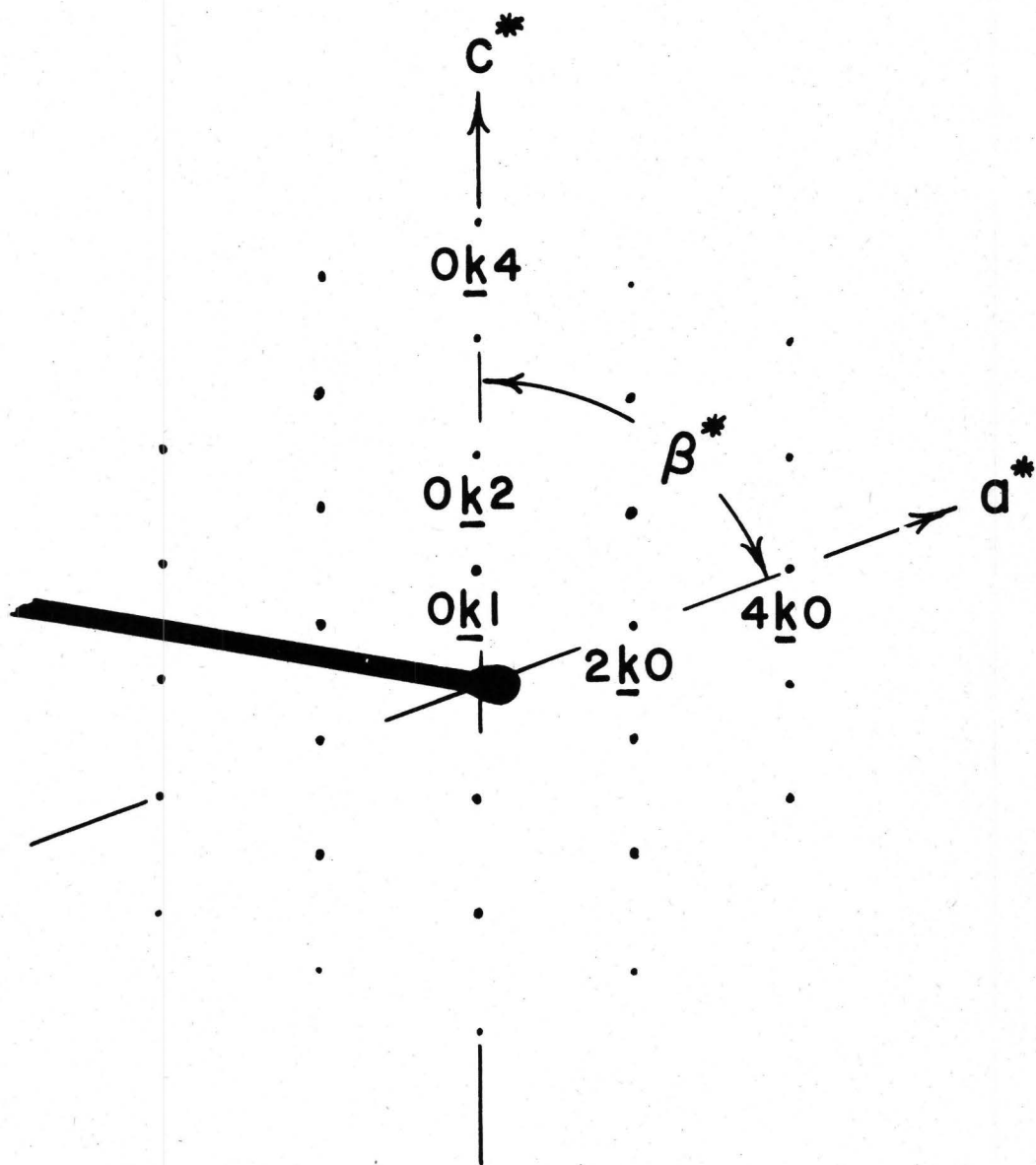


Figure 3b.--Indexed reproduction of the EDU spot pattern of colemanite shown in figure 3a.

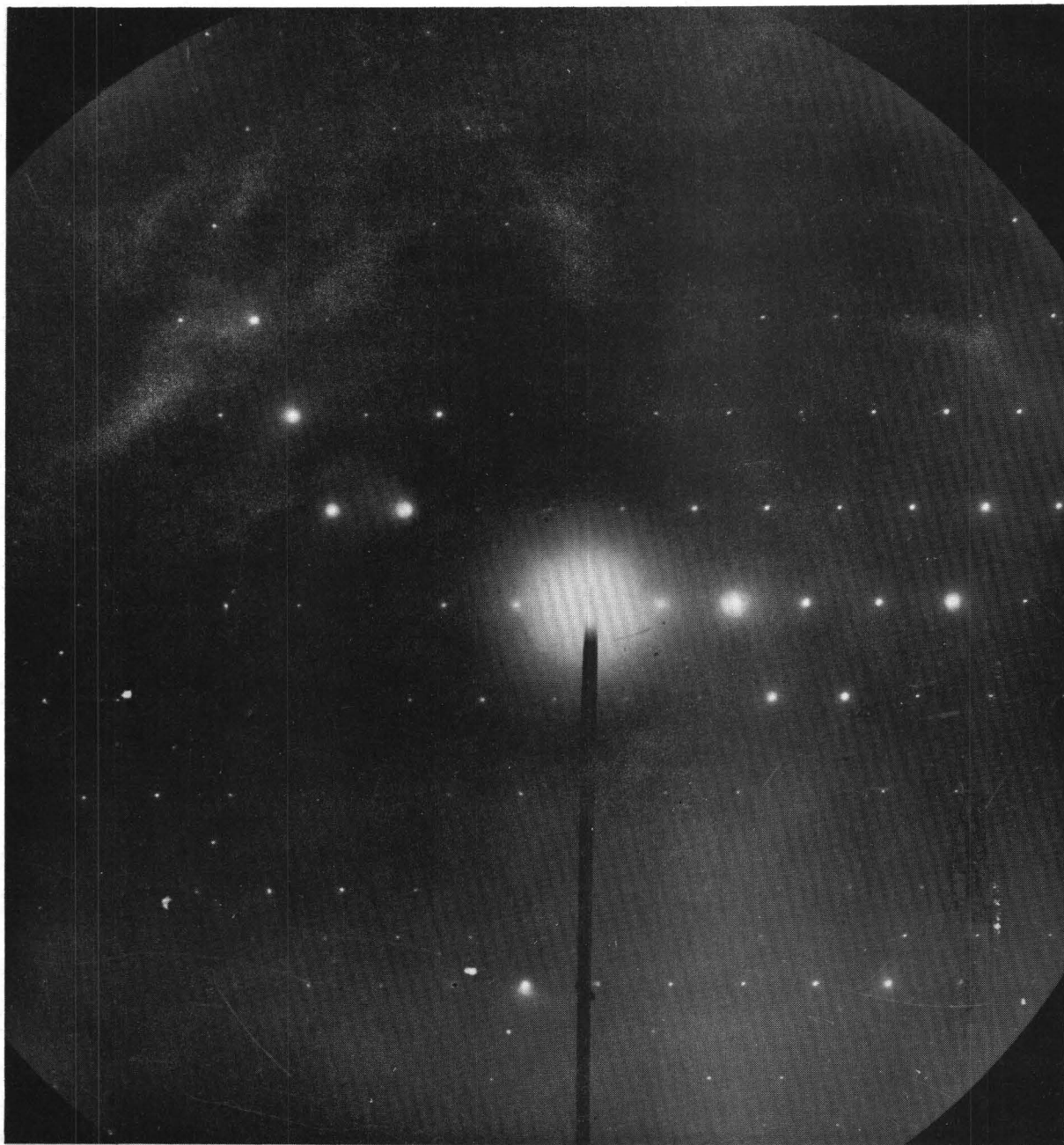


Figure 4a.--EDU spot pattern of colemanite.

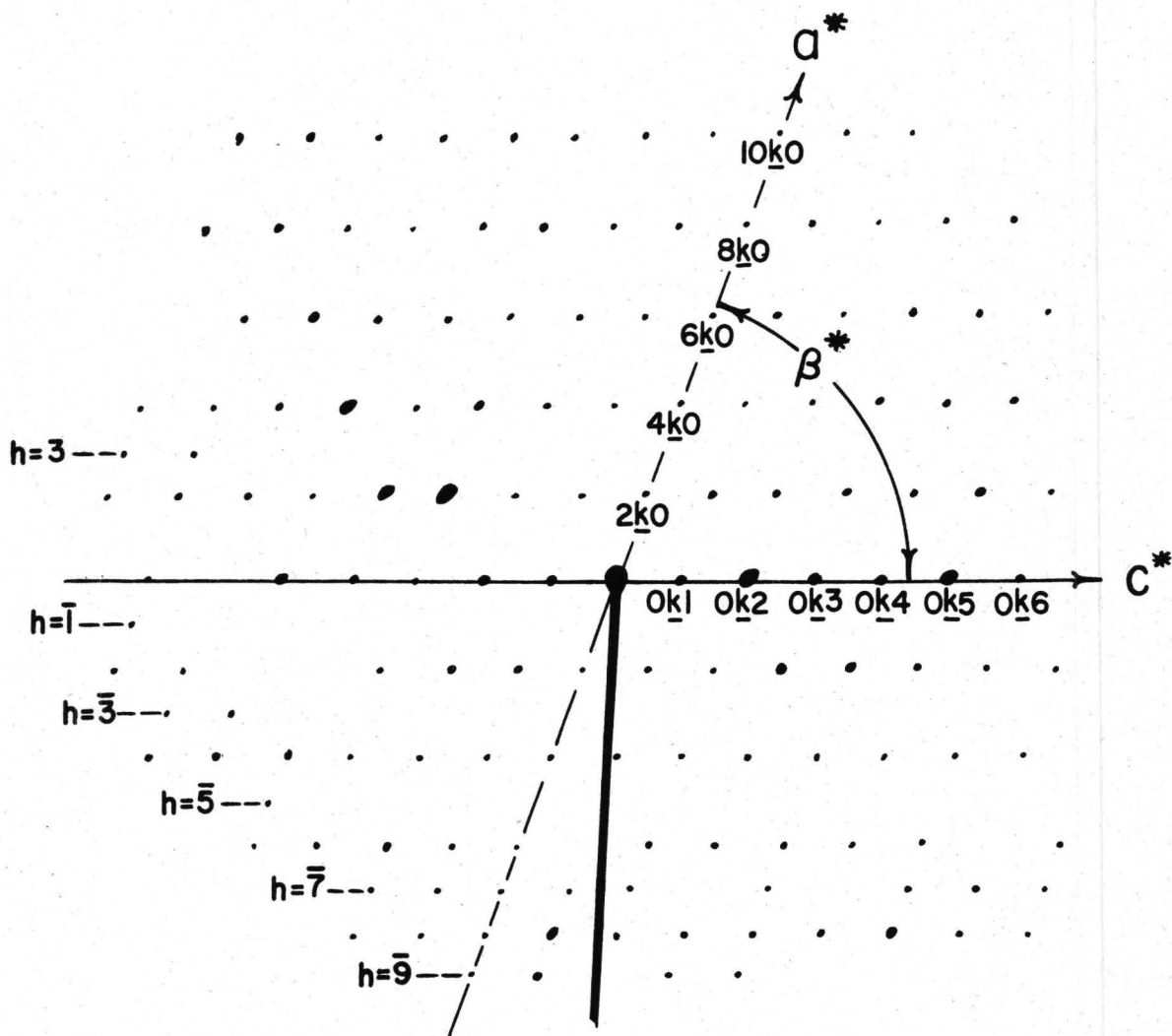


Figure 4b.--Indexed reproduction of the EDU spot pattern of colemanite shown in figure 4a.

of the sphere of reflection departs only slightly from the reciprocal lattice row $[h00]$. If the crystal is thin in the b^* direction, the reciprocal lattice points become essentially rods elongated parallel to the b^* direction. Whenever one of these rods intersects the sphere of reflection a diffracted beam is developed. Inspection of figure 5 shows that if the $h00$ reciprocal lattice points are extended as rods it is highly probable that they will penetrate the sphere since these points are nearly coincident with the trace of the sphere. If we consider the colemanite reciprocal lattice in three dimensions, it can be easily seen that with a sufficiently thin crystal a large number of rods will penetrate the sphere and give a diffraction pattern showing an extensive network of spots. Except for scale this network of spots will, geometrically, correspond very closely to the network of points in the $(h0\ell)$ reciprocal net of an ideally triperiodic colemanite crystal.

The spot patterns of colemanite are indexed with the k parameter as a variable; for example, $2k0$, where k is equal to 0, 1, $\bar{1}$, etc. This is done because it is possible that the reciprocal lattice rods in the upper levels may also extend into the sphere. The geometry of the spot pattern is not altered by extension of upper-level rods into the sphere for these rods are coincident in projection with those of the zero level. In fact, with an extremely thin crystal the reciprocal lattice points, in the rows parallel to the thin direction of the crystal, become continuous lines. In such a case we have pure two-dimensional diffraction.

The space group of colemanite is $P2_1/a-(C_{2h5})$, $h0\ell$ and $0k0$ reflections being absent when h and k are odd, respectively (Christ, 1953). Some of the higher order spots in figure 4a appear to represent "forbidden" $h0\ell$

reflections. The appearance of such reflections where h is odd can be expected if upper-level rods extend into the sphere. When a colemanite crystal is extremely thin in the b^* direction, all $hk\ell$ reflections can be expected to appear. This is shown in figure 6a, which is an SAD spot pattern of colemanite internally standardized with aluminum. The pattern shows complete rows of spots for which h is odd. The SAD pattern is indexed as shown in figure 6b. Figure 7 shows an electron micrograph of the crystal from which the SAD pattern was obtained.

Ideally these colemanite patterns should show a center of symmetry such that $I_{hkl} = I_{\bar{h}\bar{k}\bar{\ell}}$; however in practice this symmetry is not always observed. The pattern shown in figure 3a very nearly shows a center of symmetry whereas the pattern shown in figure 4a definitely does not. This lack of symmetry is attributed mainly to the variation in thickness of the cleavage fragment and to departure of the (010) face from being normal to the electron beam.

Measurement of patterns

Inasmuch as the sphere of reflection does not coincide exactly with the $(h0\ell)$ reciprocal net a slight distortion will be introduced into the spot pattern of colemanite. This distortion in terms of error in reciprocal lattice spacings may be evaluated with the aid of figure 8. The $(h0\ell)$ reciprocal lattice rod of the thin colemanite crystal will intersect the sphere at P' giving a Bragg angle of $\theta'_{h0\ell}$ corresponding to a reciprocal lattice vector $\underline{H}'_{h0\ell}$. Ideally the reciprocal lattice point $(h0\ell)$ should intersect the sphere at P giving a Bragg angle of $\theta_{h0\ell}$ corresponding to a true reciprocal lattice vector $\underline{H}_{h0\ell}$. The relation between the vectors

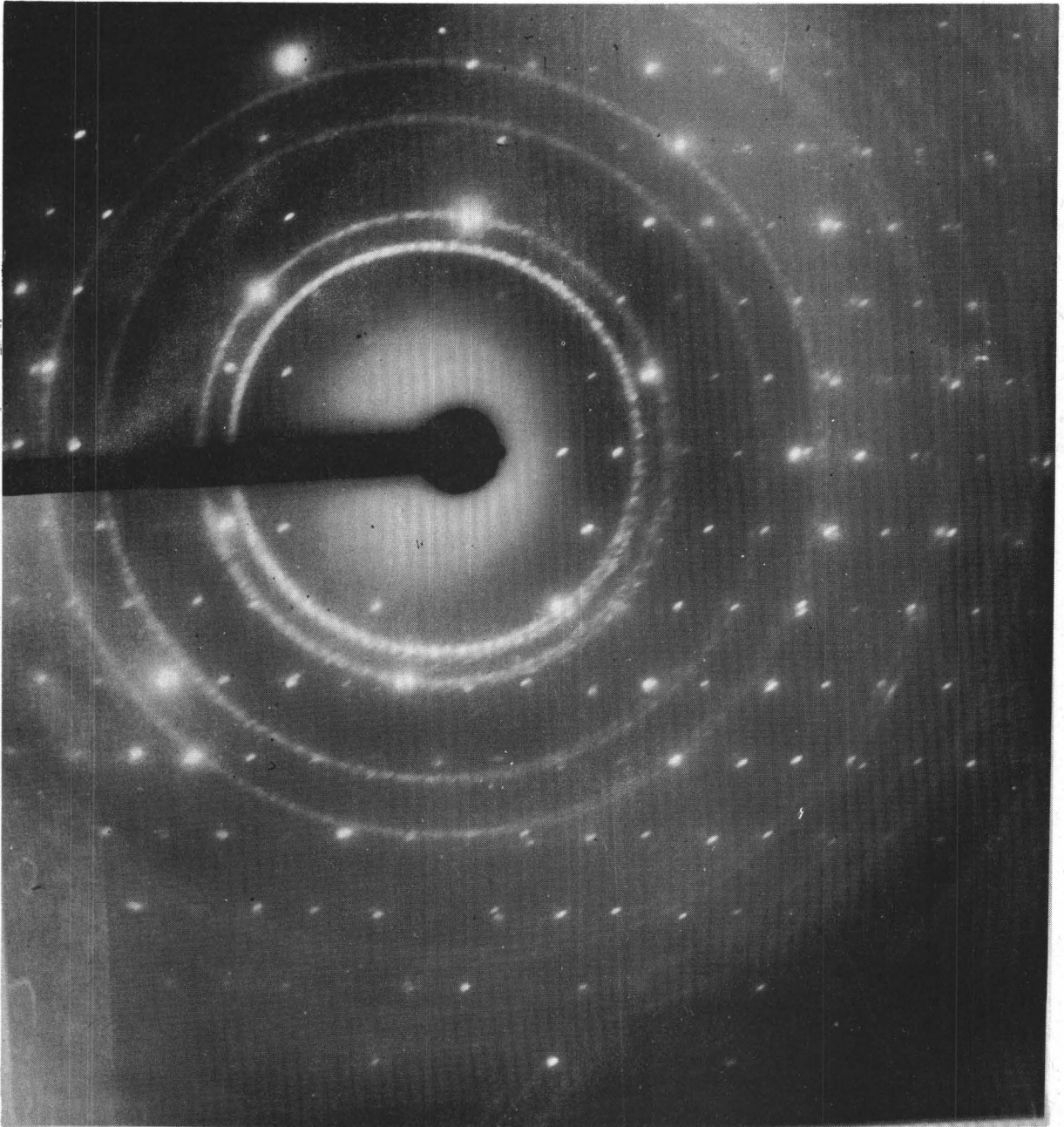


Figure 6a.--SAD spot pattern of colemanite superimposed upon the powder pattern of the internal aluminum standard.

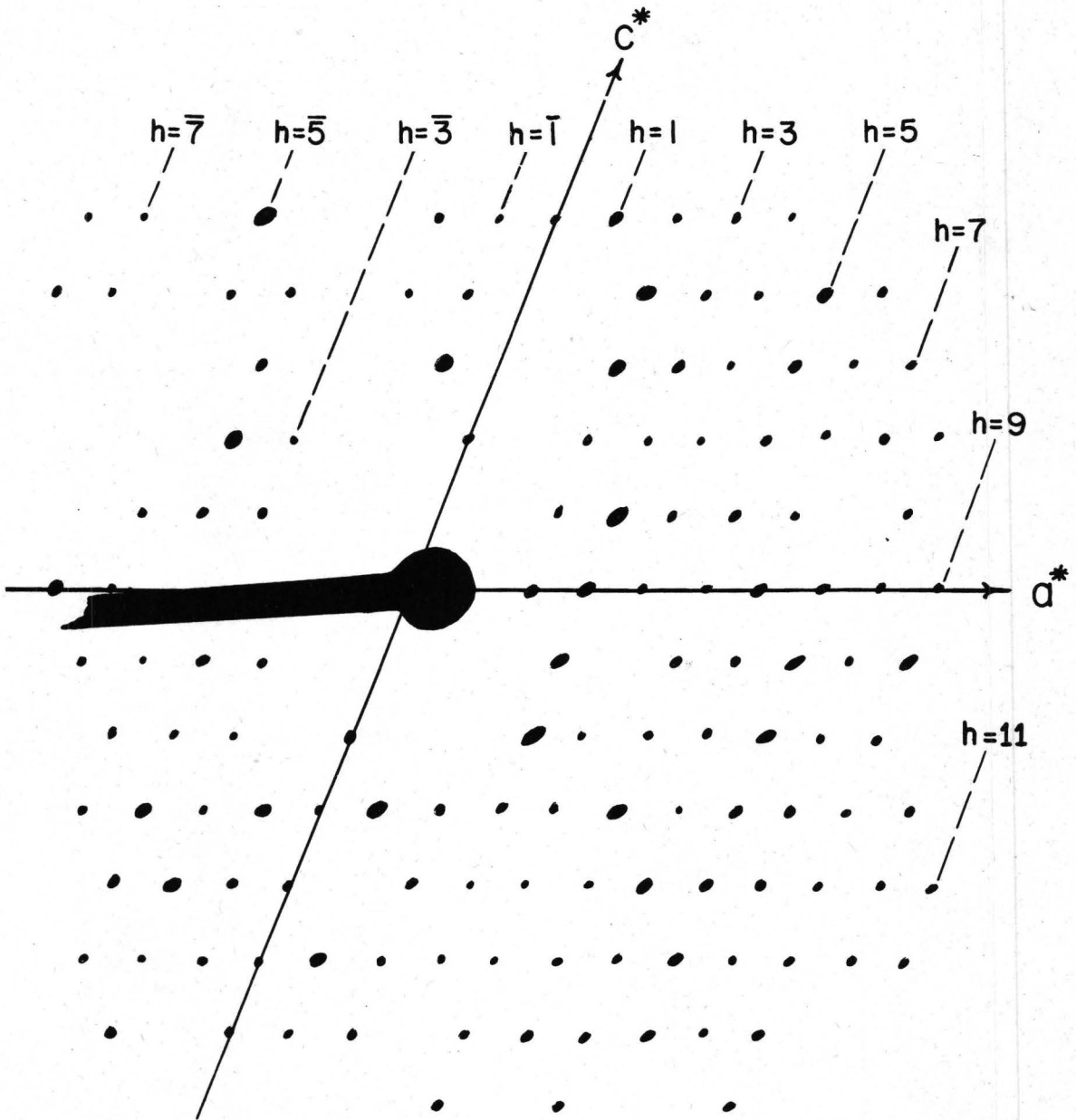


Figure 6b.--Indexed reproduction of the SAD spot pattern of colemanite shown in figure 6a.



Figure 7.--Electron micrograph of the colemanite crystal from which SAD spot pattern shown in figure 6a was made.

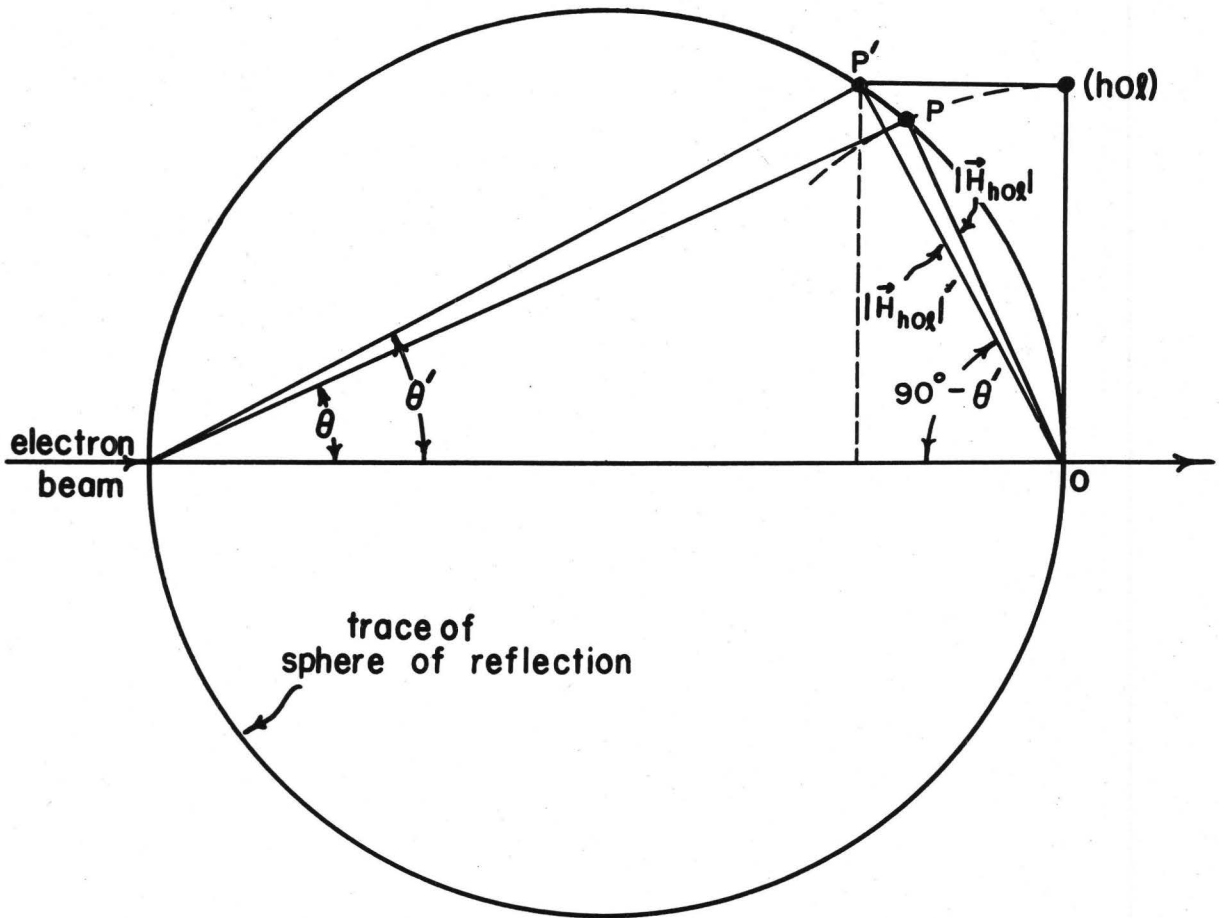


Figure 8.--The Ewald construction used to evaluate the error in reciprocal lattice spacings given by electron diffraction patterns. The curvature of the sphere of reflection is greatly exaggerated.

\underline{H}'_{hol} and \underline{H}_{hol} is given by

$$\sin (90^\circ - \theta'_{hol}) = \frac{|\underline{H}_{hol}|}{|\underline{H}'_{hol}|}$$

or

$$\cos \theta'_{hol} = \frac{|\underline{H}_{hol}|}{|\underline{H}'_{hol}|} \quad (6)$$

However

$$\cos \theta'_{hol} \cong \cos \theta_{hol} \quad (7)$$

(within a few parts per million), thus (6) on rearrangement becomes

$$|\underline{H}'_{hol}| = \frac{|\underline{H}_{hol}|}{\cos \theta_{hol}} \quad (8)$$

Relation (8) in terms of the direct lattice spacings is

$$\underline{d}'_{hol} = \underline{d}_{hol} \cos \theta_{hol} \quad (9)$$

where \underline{d}'_{hol} is the direct lattice spacing given by the spot pattern and \underline{d}_{hol} is the true direct lattice spacing.

Evaluation of direct lattice spacings from standardized EDU spot or powder patterns may be accomplished with high accuracy provided the ring diameters can be precisely measured. Rearranging (1)

we have

$$\sin \theta' = \frac{D}{4L} \frac{\cos 2\theta'}{\cos \theta'} \quad (10)$$

According to Bragg's law

$$\lambda = 2\underline{d}'_s \sin \theta' \quad (11)$$

and

$$\lambda = \frac{2d'}{x} \sin \theta'_x. \quad (12)$$

Since λ is constant we may equate (11) and (12) giving

$$\frac{d'}{x} = \frac{d'_s \sin \theta'_s}{\sin \theta'_x}. \quad (13)$$

Substitution into (13) of the value of $\sin \theta'_s$ and $\sin \theta'_x$ given by (10) gives

$$\frac{d'}{x} = \frac{\frac{d}{s} D_s \cos 2\theta'_s \cos \theta'_x}{D_x \cos 2\theta'_x \cos \theta'_s} \quad (14)$$

or for the special case of colemanite

$$\frac{d'}{h0l} = \frac{\frac{d'}{s} D_s \cos 2\theta'_s \cos \theta'_{h0l}}{D_{h0l} \cos 2\theta'_{h0l} \cos \theta'_s} \quad (15)$$

where D_{h0l} is the distance between the $h\bar{k}l$ and $\bar{h}k\bar{l}$ spots of the colemanite pattern.

But

$$\cos \theta'_{h0l} \cong \cos \theta_{h0l} \quad (7)$$

and

$$\frac{d'}{h0l} = \frac{d}{h0l} \cos \theta_{h0l}. \quad (9)$$

Also for the small Bragg angles

$$\cos 2\theta'_{h0l} \cong \cos 2\theta_{h0l}. \quad (16)$$

Most of the standard materials used in electron diffraction, for example, aluminum and β -tin, are composed of very small randomly oriented equidimensional crystals. The reciprocal lattice points of such crystals will not elongate into rods; thus the reciprocal lattice lengths $|\underline{H}'_{hkl}|$ and $|\underline{H}_{hkl}|$ of the standard material will be identical (Fig. 8). Consequently,

$$\theta'_s \equiv \theta_s, \quad (17)$$

$$\cos \theta'_s \equiv \cos \theta_s, \quad (18)$$

$$\cos 2\theta'_s \equiv \cos 2\theta_s, \quad (19)$$

and

$$\frac{d'}{s} \equiv \frac{d}{s}. \quad (20)$$

By (7), (9), (16), (18), (19), and (20), relation (15) reduces to

$$\frac{d}{h0l} = \frac{\frac{d}{s} D_s \cos 2\theta_s}{D_{h0l} \cos 2\theta_{h0l} \cos \theta_s} \quad (21)$$

or for the general case

$$\frac{d}{x} = \frac{\frac{d}{s} D_s \cos 2\theta_s}{D_x \cos 2\theta_x \cos \theta_s} \quad (22)$$

where the subscript x now refers to a material composed of crystals so thin in one direction that the reciprocal lattice points elongate into rods.

The factor $(\cos 2\theta_s)/(\cos 2\theta_x \cos \theta_s)$ in (22) usually may be disregarded since it is nearly equal to unity (within 0.2 percent) for the small θ angles encountered in the electron-diffraction method, thus (22) reduces to

$$\frac{d}{x} \cong \frac{\frac{d}{s} D_s}{D_x}. \quad (23)$$

Relation (23) was used to evaluate the direct lattice spacings given by an EDU spot pattern of colemanite similar to the one shown in figure 3a. Table 1 compares the unit-cell data obtained from the EDU pattern to those obtained

Table 1. Single-crystal data: Colemanite, $\text{CaB}_3\text{O}_4(\text{OH})_3 \cdot \text{H}_2\text{O}$, monoclinic

X-ray diffraction <u>1/</u>	Electron diffraction <u>2/</u>
$\underline{a} = 8.743 \pm 0.004 \text{ \AA}$	$\underline{a} = 8.715 \text{ \AA}$
$\underline{b} = 11.264 \pm 0.002$	--
$\underline{c} = 6.102 \pm 0.003$	$\underline{c} = 6.093$
$\underline{d}_{200} = 4.105 \text{ \AA (calc.)}$	$\underline{d}_{200} = 4.094 \text{ \AA (meas.)}$
$\underline{d}_{001} = 5.730 \text{ (calc.)}$	$\underline{d}_{001} = 5.726 \text{ (meas.)}$
$\underline{d}_{20\bar{1}} = 4.063 \text{ (calc.)}$	$\underline{d}_{20\bar{1}} = 4.050 \text{ (meas.)}$
$\beta = 110^\circ 07' \pm 05'$	$\beta = 110^\circ 00'$
Space group $\underline{P}2_1/\underline{a} - (\underline{C}_{2h}^5)$	--

1/ Christ, 1953

2/ Measurements are taken from an EDU spot pattern similar to the one shown in figure 3a.

by X-ray methods (Christ, 1953). The β angle for the electron-diffraction value was determined by triangulation.

If accuracy of better than 0.2 percent is desired, $\frac{d}{x}$ must be calculated using relation (22). The factor $(\cos 2\theta_s)/(\cos 2\theta_x \cos \theta_s)$ for a given direct lattice spacing may be routinely determined from a graph made by plotting the value of $(\cos 2\theta_s)/(\cos 2\theta_x \cos \theta_s)$ for several direct lattice spacings against the direct lattice spacings. Figure 9 shows such a graph which is computed for use with electron-diffraction patterns that are photographed at a potential of 50 kv ($\lambda = 0.0534$ A) and standardized with the (501) reflection of β -tin ($\frac{d}{501} = 1.0950$ A, Swanson and Tatge, 1953, p. 25). The graph is used in the following way. A $(\frac{d}{x})$ approx. is calculated using relation (23). For this value the corresponding value of $(\cos 2\theta_s)/(\cos 2\theta_x \cos \theta_s)$ is found on the graph and then multiplied into $(\frac{d}{x})$ approx. to give a more accurate value of $\frac{d}{x}$. By this means it is possible to calculate $\frac{d}{x}$ with an accuracy of better than 0.01 percent assuming, of course, that $\frac{d}{s}$, D_s and D_x are as accurately known. Usually spot patterns cannot be measured with sufficient precision to warrant use of the graph. Powder patterns, on the other hand, can sometimes be measured with great precision; thus the need for the more accurate evaluation of $\frac{d}{x}$ furnished by the graph is apparent.

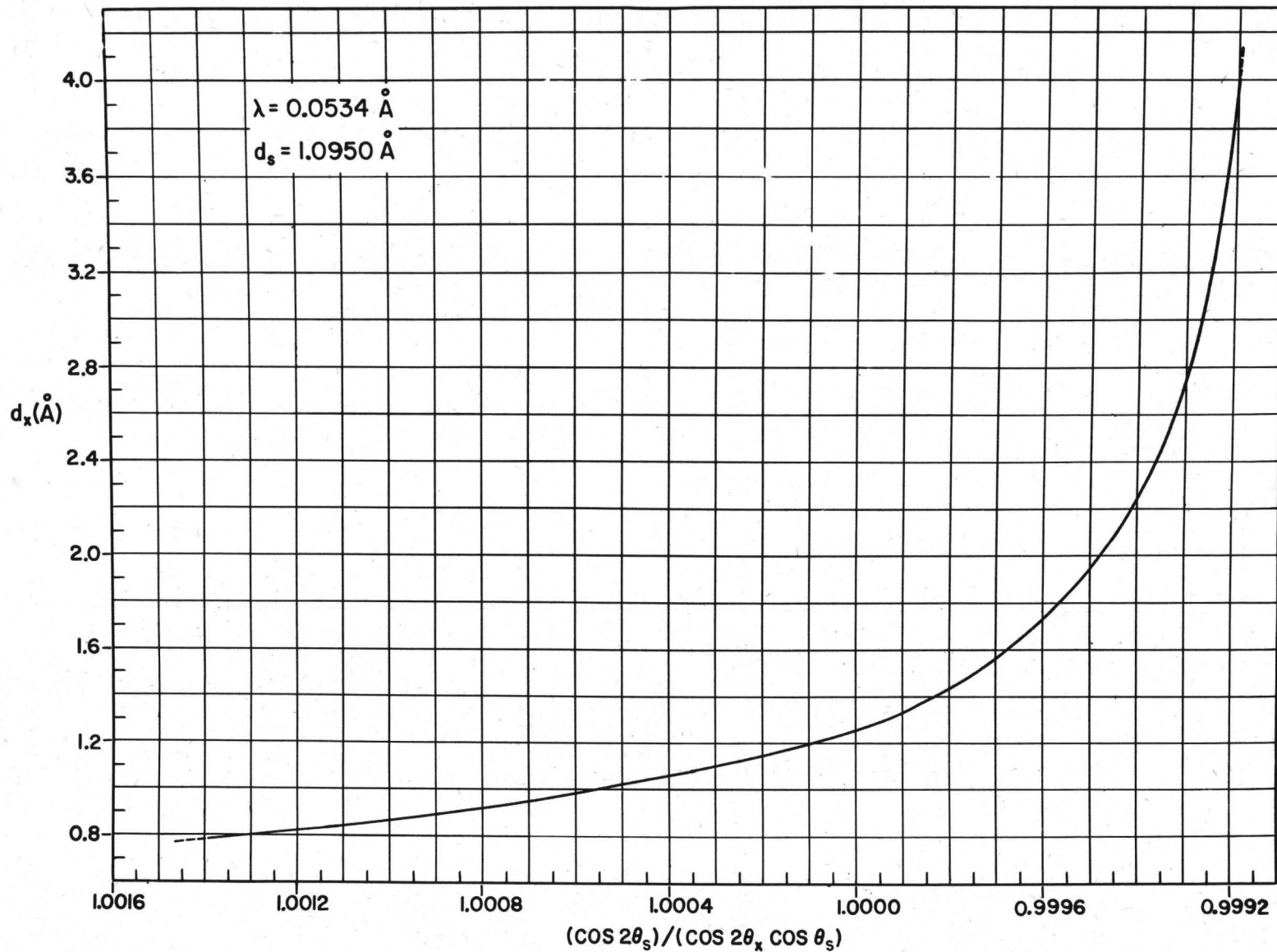


Figure 9.--Graph for evaluating the factor $(\cos 2\theta_s) / (\cos 2\theta_x \cos \theta_s)$ for a given direct lattice spacing. The graph is computed for electron-diffraction patterns that are photographed at a potential of 50 kv ($\lambda = 0.0534 \text{ \AA}$) and standardized with the (501) reflection of β -tin ($d_{501} = 1.0950 \text{ \AA}$).

ANALYSIS OF SINGLE-CRYSTAL PATTERNS OF KClO_3

Interpretation of patterns

KClO_3 is monoclinic and in its pure form crystallizes from solution as thin tablets on (001). (See Buckley 1951, p. 544.) Specimens of this material were prepared by placing a drop of very dilute aqueous KClO_3 solution on a collodion mount which had been previously coated with aluminum or with β -tin. After the mounts were air-dried, they were oriented in the electron-diffraction unit so that (001) was approximately normal to the electron beam. The position of the specimen mount and the KClO_3 crystal in relation to the electron beam is shown in figure 10.

Ten internally standardized EDU spot patterns were made of this material, eight of which were suitable for measurement. One of these patterns is shown in figure 11a; the pattern is indexed as shown in figure 11b.

The method of interpreting the KClO_3 patterns can be visualized with the aid of figure 12 which represents a portion of the KClO_3 reciprocal lattice through the origin and perpendicular to the b -axis. If the crystal is sufficiently thin in the c^* direction, the reciprocal lattice rods will be elongated parallel to c^* and many of them will penetrate the sphere of reflection. It can be seen with the aid of figure 12 that dimensions of the spot pattern obtained from the KClO_3 crystal will be very nearly proportional to those of a projection of the (hk0) reciprocal net onto the a - b plane of the crystal. The deviation from true proportionality arises because the sphere of reflection does not quite coincide with the a - b plane.

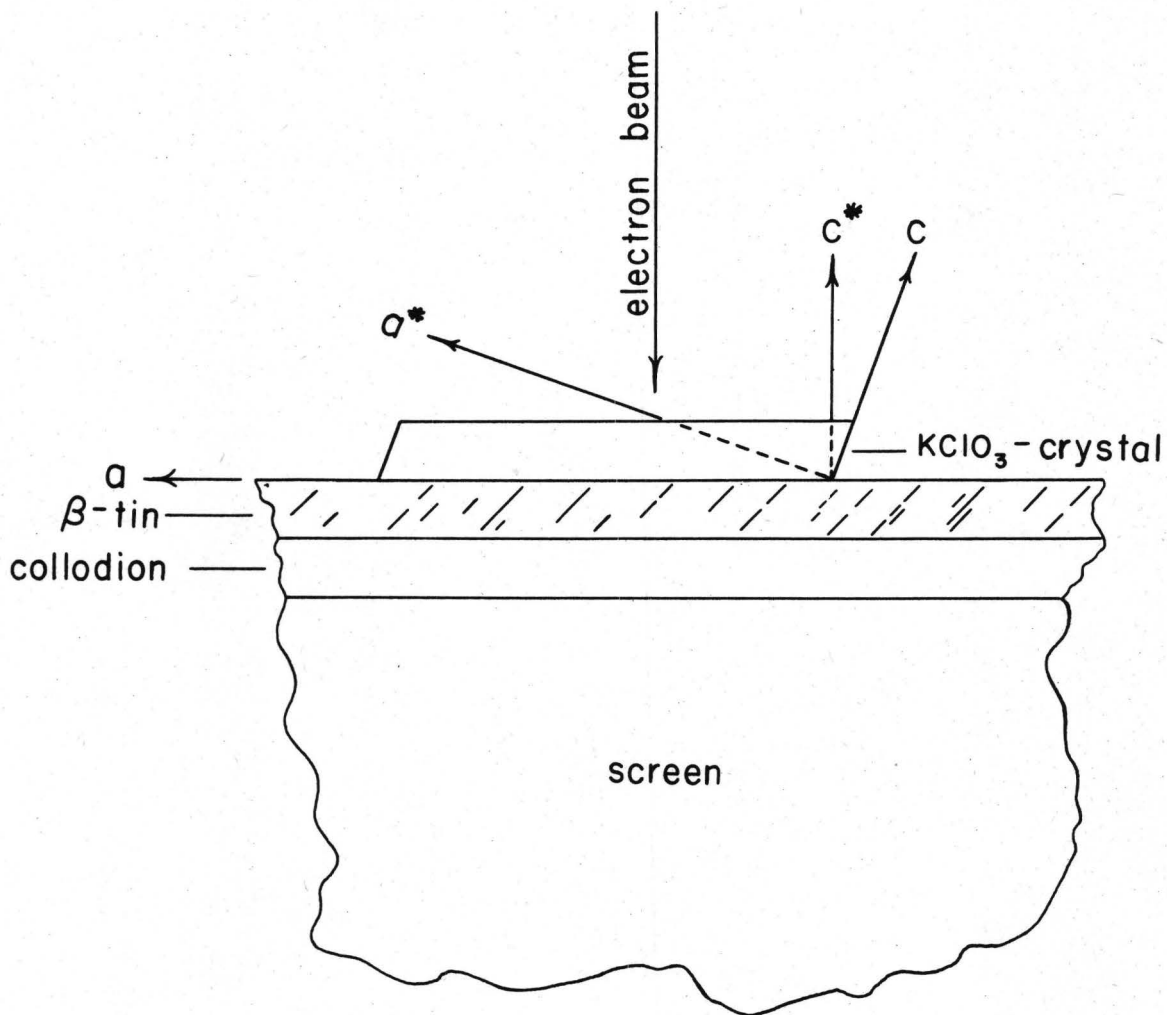


Figure 10.--The position of the specimen mount and the KClO_3 crystal in relation to the electron beam.

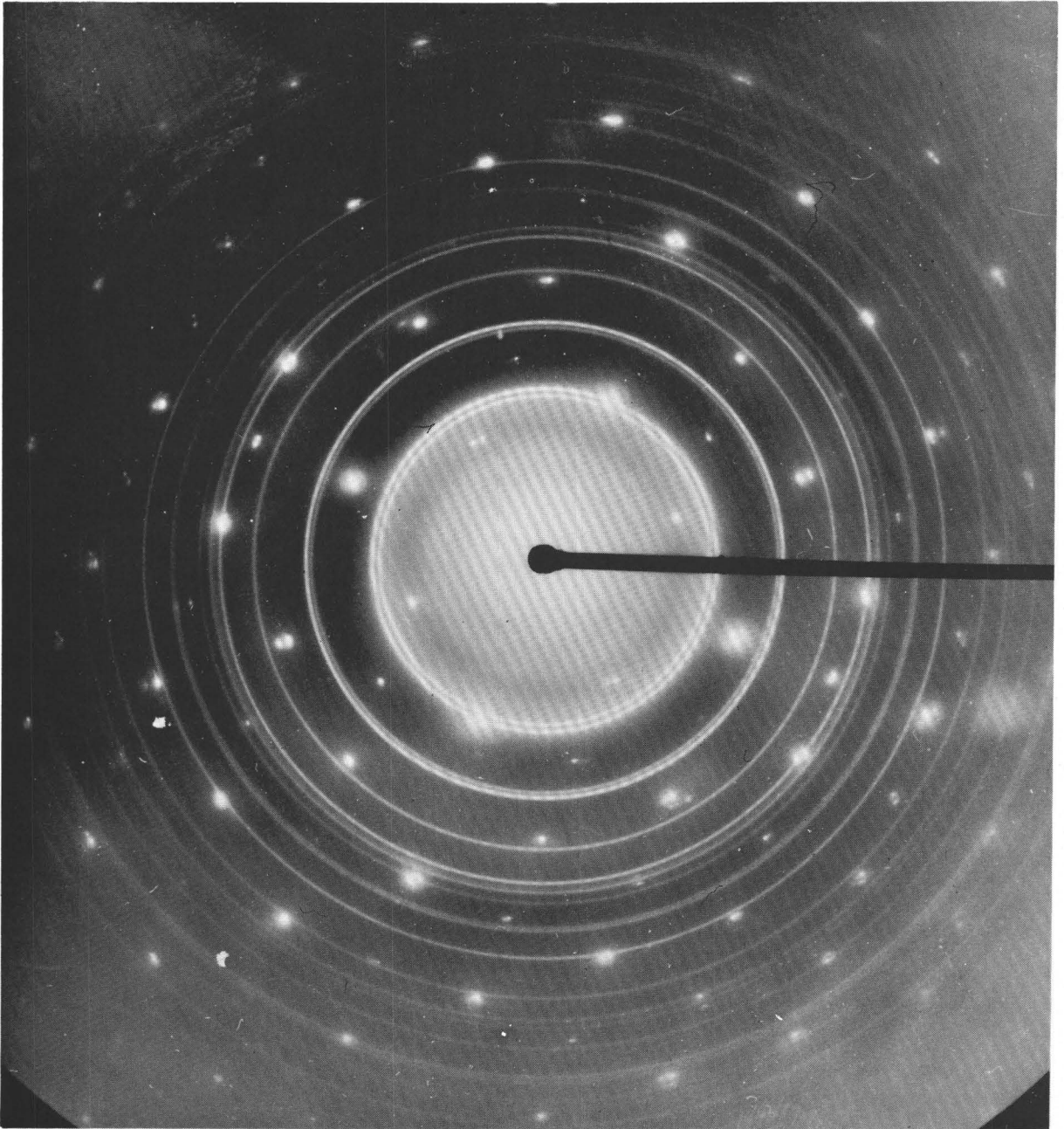


Figure 11a.--EDU spot pattern of KClO_3 (h0l) superimposed upon the powder pattern of the internal β -tin standard.

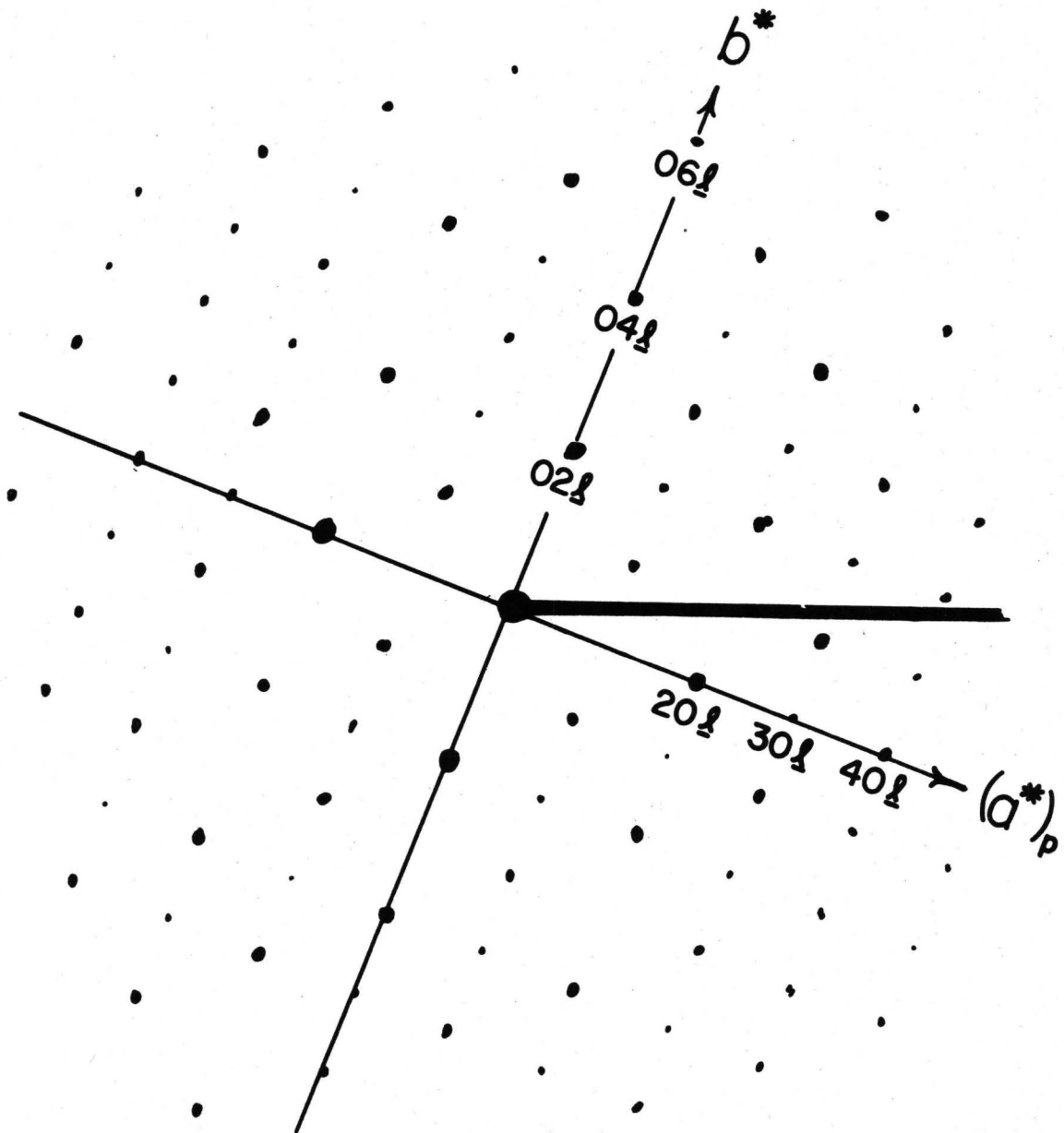


Figure 11b.--Indexed reproduction of the EDU spot pattern of KClO_3 shown in figure 11a.

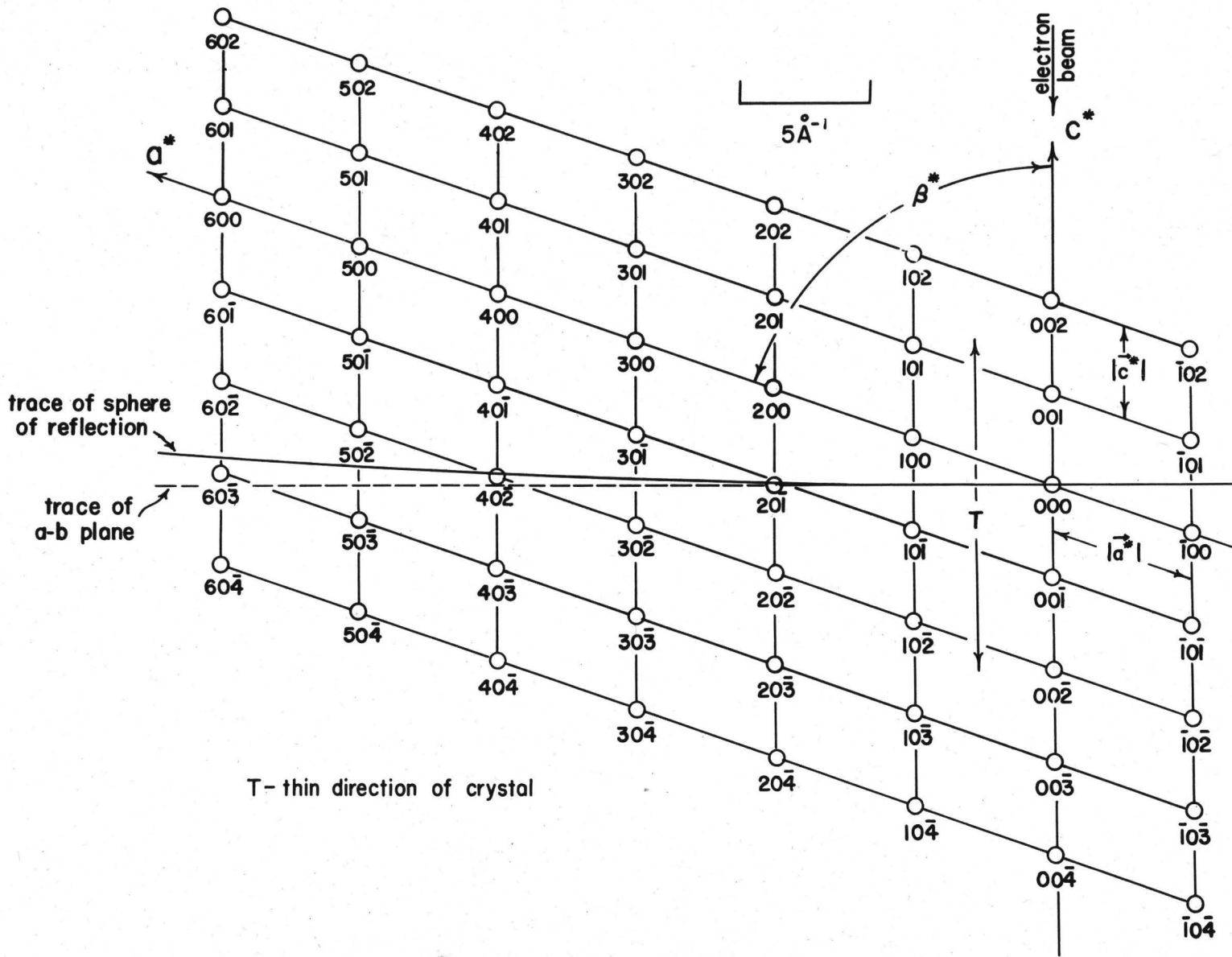


Figure 12.--Ewald construction showing a portion of the section of the KClO_3 reciprocal lattice through the origin and perpendicular to the b -axis ($\lambda = 0.0534 \text{ \AA}$).

The spots along the positive $(a^*)_p$ direction (projected a^* direction) in the $KClO_3$ spot pattern (fig. 11a) are indexed as $20\bar{l}$, $30\bar{l}$, and $40\bar{l}$ (fig. 11b); and correspond to the intersection of the sphere by one or more rods in the reciprocal lattice rows $[20\bar{l}]$, $[30\bar{l}]$, and $[40\bar{l}]$, respectively. Spots having the indices $10\bar{l}$ and $50\bar{l}$ do not appear in the spot pattern indicating that none of the rods in the reciprocal lattice rows $[10\bar{l}]$ and $[50\bar{l}]$ penetrate the sphere.

The space group of $KClO_3$ is $P2_1/m - (C_{2h}^2)$, $Ok0$ reflections being absent when k is odd (Zachariasen, 1929, p. 501). The very weak spots indexed as $01\bar{l}$, $03\bar{l}$ and $05\bar{l}$ (figs. 13a and 13b) arise because reciprocal lattice rods from the upper $Ok\bar{l}$ levels penetrate the sphere. This can be readily understood from figure 14 which shows a portion of the section of the $KClO_3$ reciprocal lattice, through the origin and perpendicular to the a -axis.

Measurement of patterns

The lattice spacings given by the $KClO_3$ spot pattern may be evaluated with the aid of figure 15 which shows a projection of the $(hk0)$ reciprocal net of $KClO_3$ onto the a - b plane. Consider the reciprocal lattice vector \underline{H}_{hk0} to any point $hk0$. The length of its projection onto the a - b plane is given by

$$|\underline{H}_{hk0}|_p^2 = [h\underline{a}^* \cos(90^\circ - \beta^*)]^2 + [k\underline{b}^*]^2$$

or

$$|\underline{H}_{hk0}|_p = \left(\frac{\sin^2 \beta}{d_{h00}^2} + \frac{1}{d_{0k0}^2} \right)^{\frac{1}{2}} \quad (24)$$

where $|\underline{H}_{hk0}|_p$ is the reciprocal lattice spacing given by projection of the

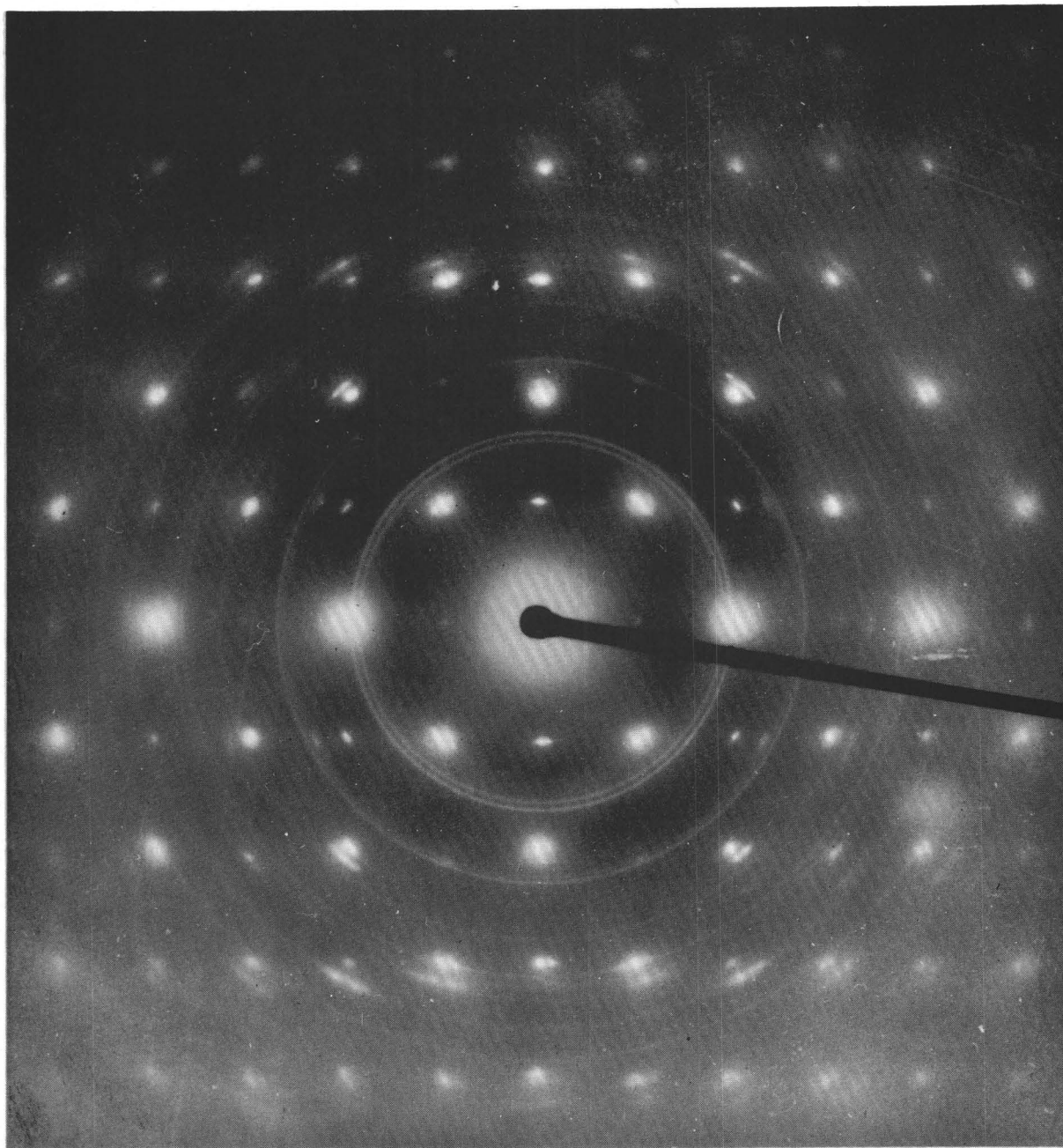


Figure 13a.--EDU spot pattern of KClO_3 ($0k\bar{l}$) superimposed upon the powder pattern of the internal β -tin standard.

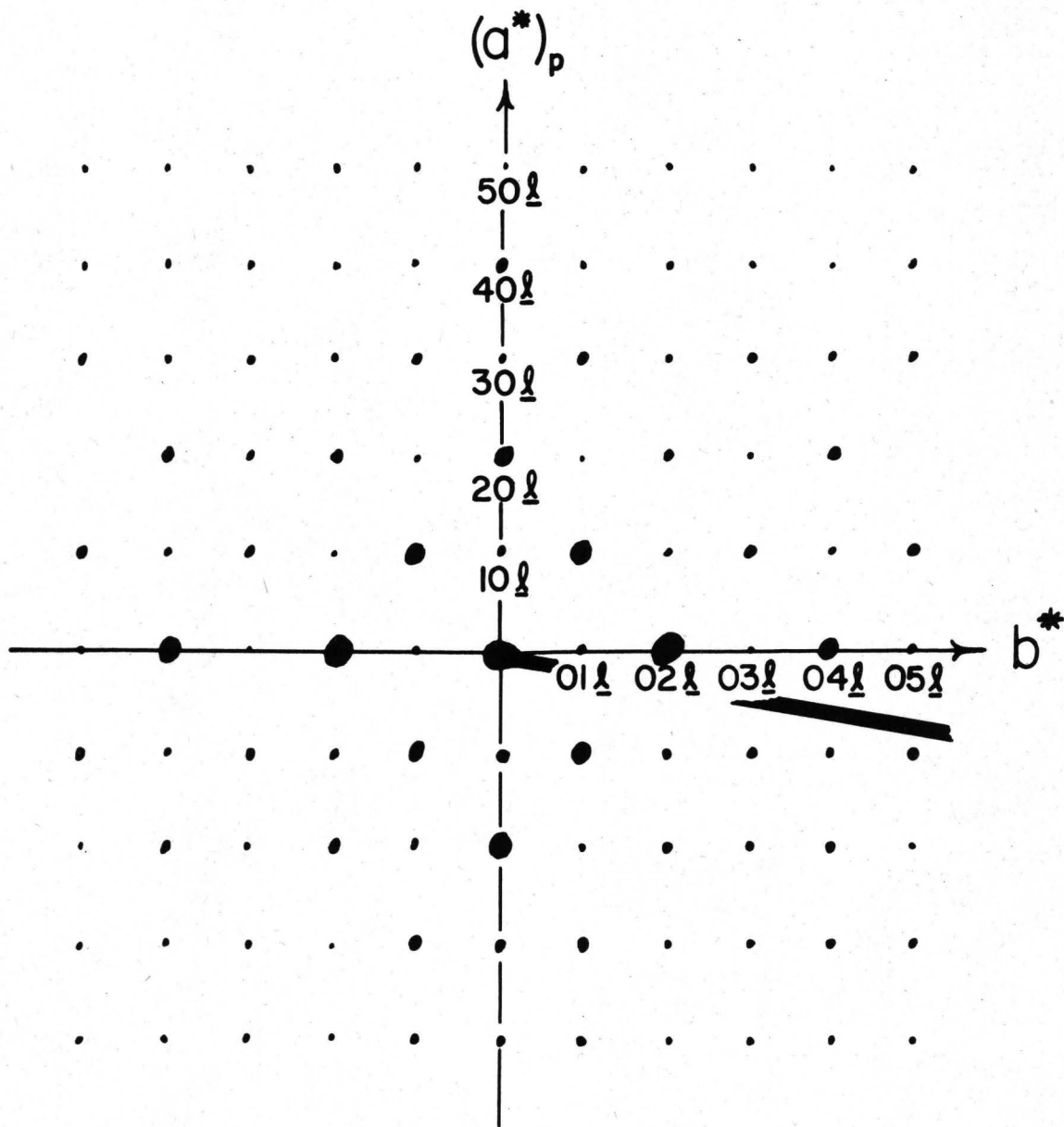


Figure 13b.--Indexed reproduction of the EDU spot patterns of KClO_3 shown in figure 13a.

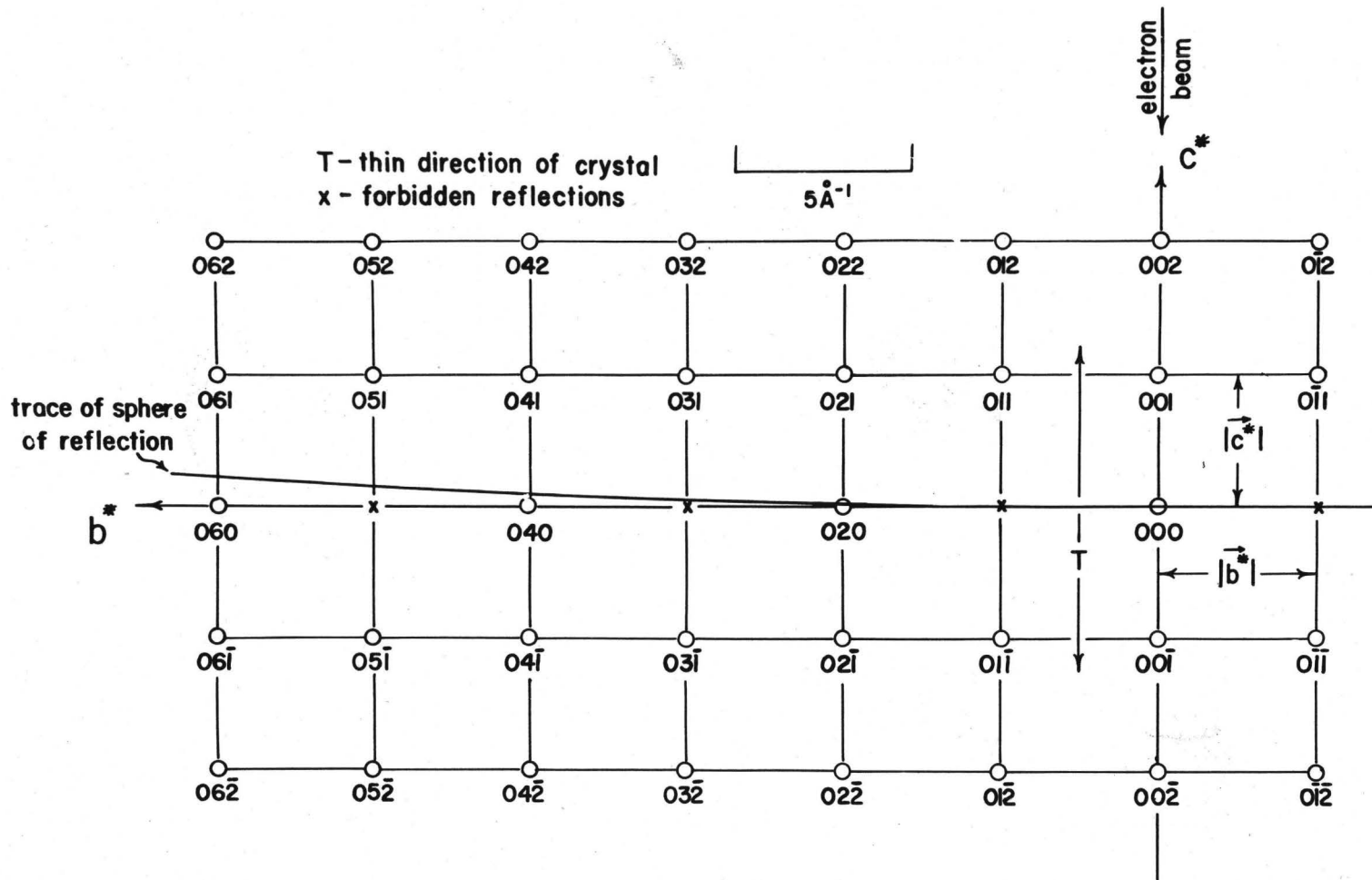


Figure 14.--Ewald construction showing a portion of the section of the KC10_3 reciprocal lattice through the origin and perpendicular to the \underline{a} -axis ($\lambda = 0.0534 \text{ \AA}$).

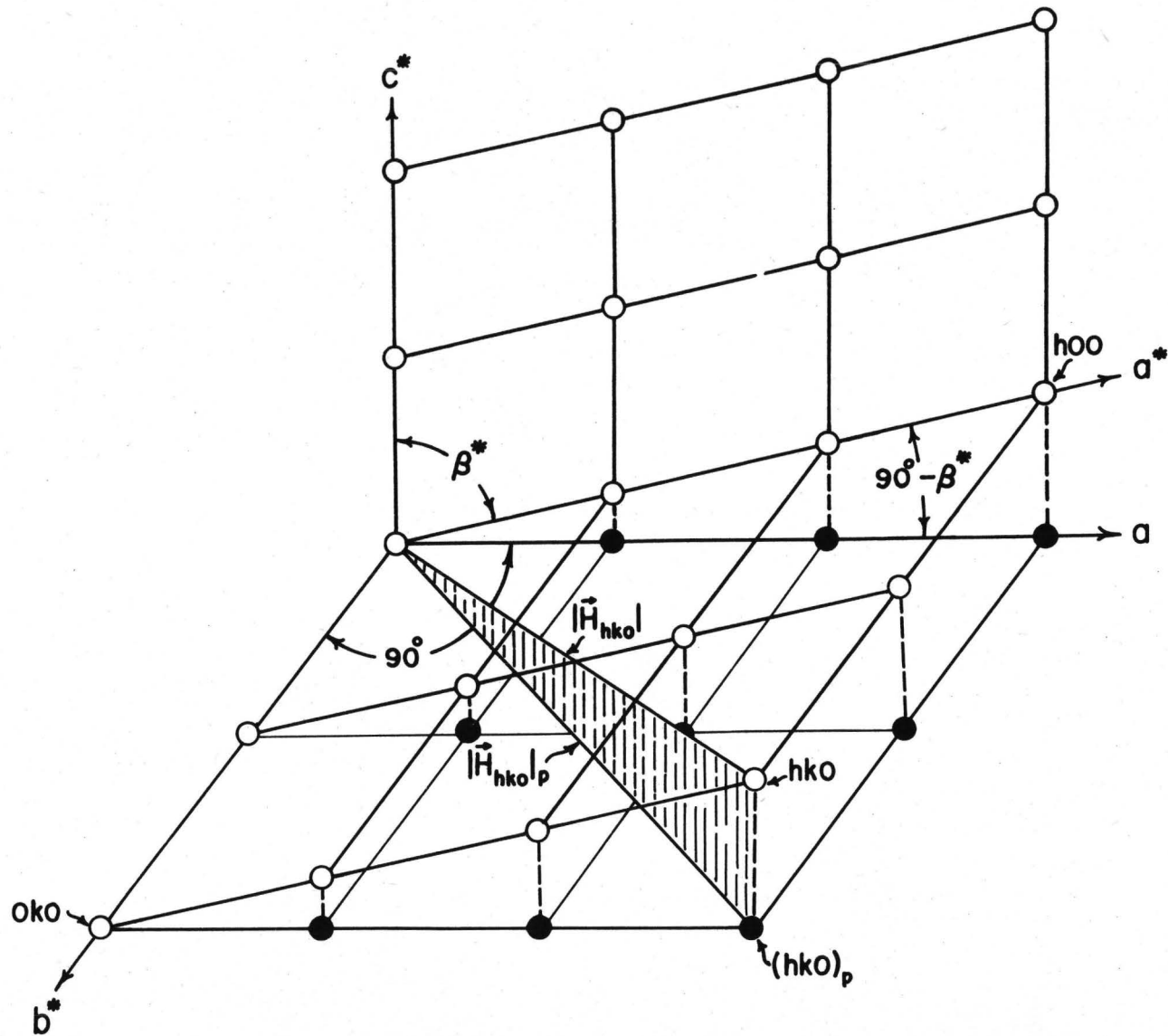


Figure 15.--Geometrical construction used to evaluate the projection of the $(hk0)$ reciprocal net of KClO_3 onto the a - b plane.

vector \underline{H}_{hk0} . In terms of the direct lattice (24) becomes

$$(\underline{d}_{hk0})_p = \frac{1}{\left(\frac{\sin^2 \beta}{\underline{d}_{h00}^2} + \frac{1}{\underline{d}_{0k0}^2} \right)^{\frac{1}{2}}} \quad (25)$$

where $(\underline{d}_{hk0})_p$ is the projection of \underline{d}_{hk0} and is very nearly equal to the spacing given by the spot pattern. If $h = 1$ and $k = 0$, (25) reduces to

$$(\underline{d}_{100})_p = \underline{a}. \quad (26)$$

If $h = 0$ and $k = 1$, (25) reduces to

$$(\underline{d}_{010})_p = \underline{b}. \quad (27)$$

Relation (23) gives a satisfactory method of evaluating direct lattice spacings from measurements of spot patterns. Applying this relation specifically to the KClO_3 case we have

$$(\underline{d}_{hk0})_p \approx \frac{\underline{d}_s D_s}{D_{(hk0)}_p} \quad (28)$$

where $D_{(hk0)}_p$ is the distance between the $hk\underline{l}$ and $\bar{h}\bar{k}\underline{l}$ spots.

Planes of symmetry appear in all the KClO_3 spot patterns showing that the γ^* angle is 90° . Table 2 gives the values of the \underline{a} and \underline{b} unit-cell constants of KClO_3 obtained from measurement of the higher order $h0\underline{l}$ and $0k\underline{l}$ reflections of eight spot patterns. One pattern (No. 246) gives an exceptionally low value for \underline{b} . This was probably the result of a large deviation of the \underline{a} - \underline{b} plane of the KClO_3 crystal from 90° to the electron beam. Table 3 compares the average values of \underline{a} and \underline{b} obtained from the EDU spot patterns to the X-ray values (Zachariasen, 1929).

Table 2. Values of the a and b unit-cell constants obtained from measurement of the higher order reflections of eight $KClO_3$ EDU single-crystal patterns.

<u>a</u>	Pattern No.	<u>b</u>	Pattern No.
4.64 ₈ A	233	5.54 ₂ A	233
4.66 ₄	233	5.54 ₈	233
4.66 ₀	234	5.54 ₈	234
4.67 ₂	234	5.56 ₈	234
4.66 ₆	235	5.55 ₆	235
4.67 ₂	235	5.56 ₆	237
4.65 ₆	237	5.56 ₈	237
4.65 ₈	237	5.58 ₂	245
4.63 ₈	245	5.57 ₂	245
4.65 ₄	246	5.57 ₀	245
4.66 ₄	246	5.49 ₀ ^{1/}	246
4.65 ₀	402	5.57 ₀	402
4.67 ₂	404	5.55 ₆	404
Average 4.659 A		Average 5.562 A	
Average deviation 0.008 A		Average deviation 0.010 A	

^{1/} This low value is not included in the average. It probably arises because the a-b plane of the crystal deviates appreciably from being normal to the electron beam. Average values for a and b are taken as being closer approximations to the truth than maximum values of a and b. It is considered that the errors are due principally to causes other than deviation of the a-b plane from the ideal position (except in Pattern No. 246).

Table 3. Single-crystal data: KClO_3 , monoclinic.

X-ray diffraction <u>1/</u>	Electron diffraction <u>2/</u>
$\underline{a} = 4.656 \pm 0.004 \text{ \AA}$	$\underline{a} = 4.659 \pm 0.008 \text{ \AA}$
$\underline{b} = 5.596 \pm 0.005$	$\underline{b} = 5.562 \pm 0.010$
$\underline{c} = 7.099 \pm 0.007$	
$\underline{d}_{100} = 4.386 \text{ \AA (calc.)}$	
$\underline{d}_{10\bar{1}} = 4.409 \text{ (calc.)}$	
$\beta = 109^\circ 38' \pm 05'$	
Space group - $\underline{P}2_1/\underline{m}$ - ($\underline{C}2h^2$)	

1/ Zachariasen (1929), spacings have been converted from kX units to angstrom units.

2/ Average of eight EDU spot patterns.

No diffraction patterns of KClO_3 were obtained with the electron microscope because the heat generated by the beam decomposed the crystals. Some decomposition also occurred in the electron-diffraction unit. The pattern shown in figure 13a shows some effects of decomposition including broadening of the spots. The EDU pattern shown in figure 16a was taken after a KClO_3 single crystal had been centered in the beam for ten minutes. This pattern shows an almost complete decomposition of KClO_3 to KCl and represents a large number of KCl crystals oriented with a cube face parallel to the collodion film (arbitrarily assigned as the (001) face in figure 16b). The spots are more or less extended arcs having the most intense blackening in the centers and a sharp decrease in blackening towards their extremities. This shows that the KCl crystals are also oriented in azimuth; that is, in the plane of the film. The $hk0$ reflections with h and/or k odd do not appear in the KCl pattern shown in figure 16a. This is because the scattering powers of the potassium and chloride ions are almost exactly equal and therefore only $hk\ell$ reflections where h , k , and $\ell = 2n$ appear. The single-crystal pattern of KCl thus appears to be that of a primitive cell with $a(\text{apparent}) = a/2(\text{real})$. Measurement of the KCl pattern yields a value of $d_{200} = 3.15 \text{ \AA}$. Swanson and Tatge (1953, p.66) find d_{200} for KCl to be 3.146 \AA .

DISCUSSION

It is clear that useful crystallographic data can be obtained from the electron-diffraction study of single crystals, as shown by the results obtained on colemanite and KClO_3 . For these substance unit-cell constants accurate to a few parts per thousand were obtained.

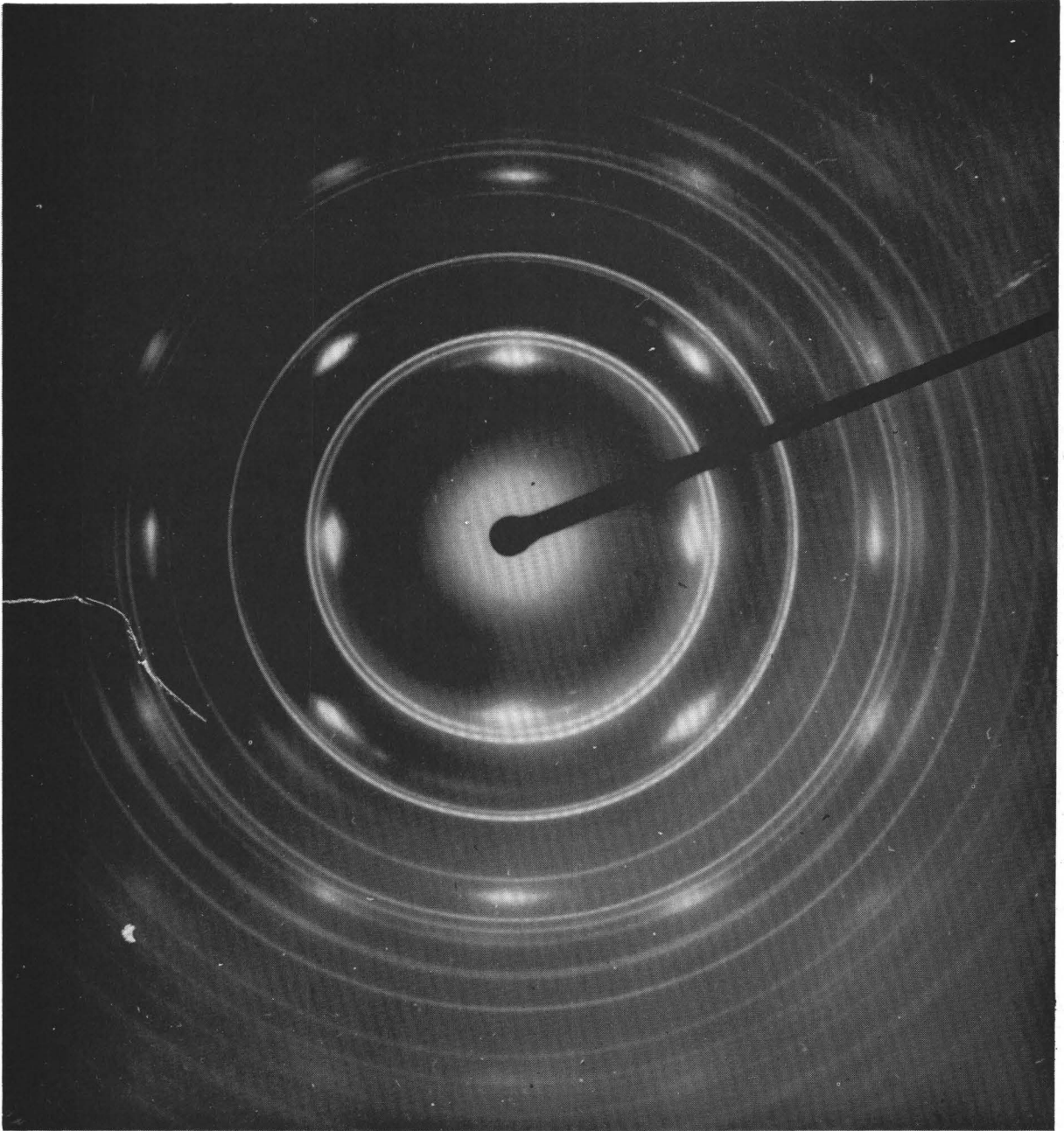


Figure 16a.--EDU pattern taken after a single crystal of KClO_3 had been centered in the electron beam for ten minutes. The rings are those of the internal β -tin standard.

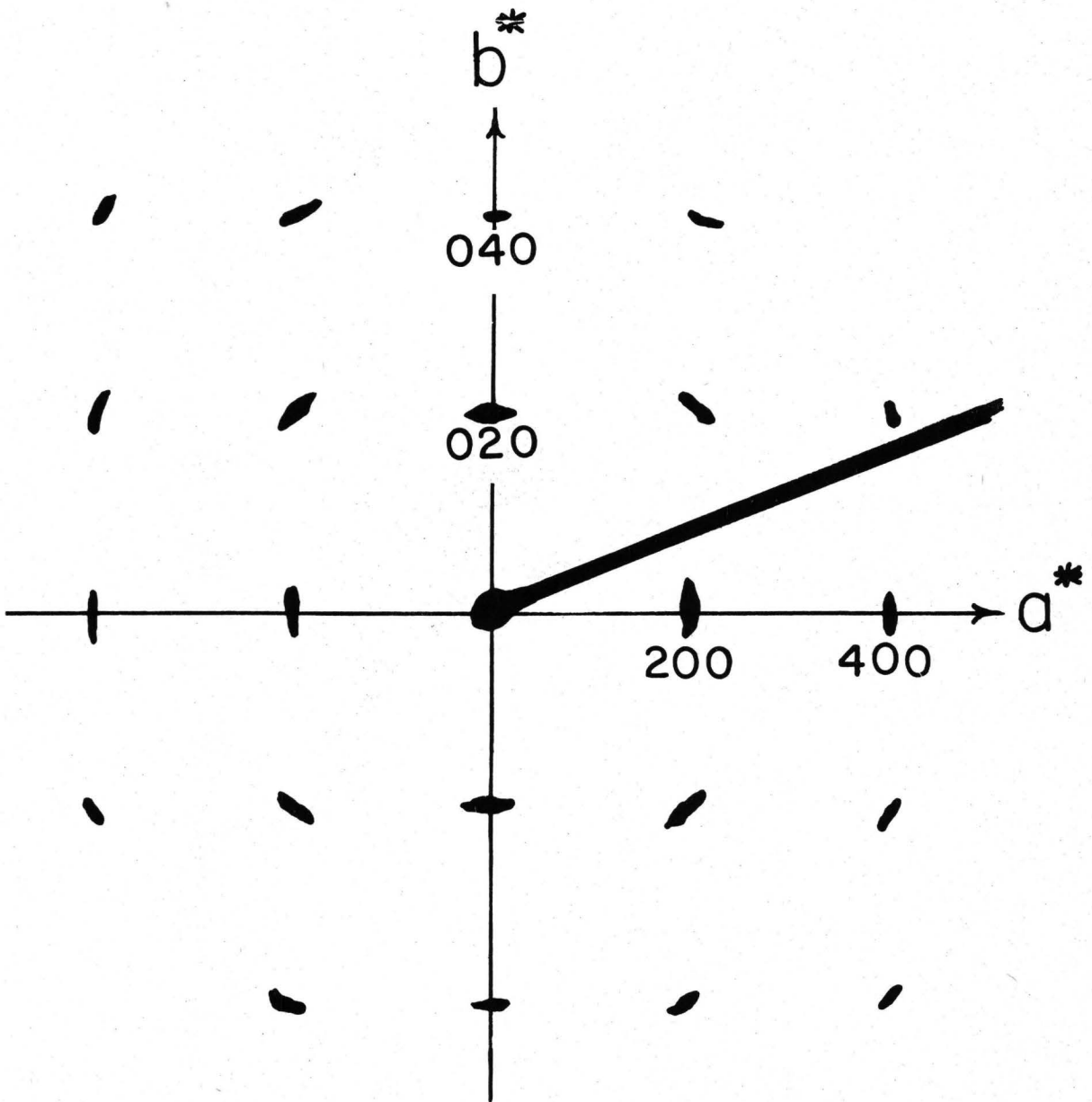


Figure 16b.--Indexed reproduction of the EDU pattern shown in figure 16a.

It is to be emphasized that we have been here dealing with an experimental arrangement in which the electron beam is normal to a crystal lying on a cleavage or natural face. From reciprocal lattice theory this means that if the crystal is lying on a face (hkl) the beam is parallel to the reciprocal lattice vector \underline{H}_{hkl} . The vectors normal to \underline{H}_{hkl} , and lying in the plane of the face, are, in the general case, direct lattice vectors. The principal reciprocal lattice vectors may or may not lie in this plane, depending upon the crystal system, a fact which must be taken into account in the interpretation of the diffraction patterns. A thin monoclinic crystal lying on the (001) face is an example in which the principal direct lattice and reciprocal lattice vectors do not lie in the same plane. We have treated this case in some detail for $KClO_3$. The interpretation given for this substance may be readily expanded for the most general case, the triclinic.

The electron-diffraction single-crystal experiment is to be contrasted with the X-ray diffraction single-crystal experiment. With the former the diffraction spots give directly the projected quantities $|\underline{H}_{hkl}|_p$ whereas with the latter the diffraction spots give directly the quantities $|\underline{H}_{hkl}|$. In the case of orthogonal crystals $|\underline{H}_{hkl}|_p \equiv |\underline{H}_{hkl}|$.

The procedures used to interpret the single-crystal patterns of colemanite and $KClO_3$ may be applied to the interpretation of patterns obtained from crystals belonging to any crystal system. Table 4 gives the crystallographic data that may be obtained directly from spot patterns of crystals belonging to the six crystal systems. Spot patterns obtained from crystals which orient other than on (100) , (010) , or (001) would have to be indexed assuming orientation upon a pinacoidal face and then if possible a suitable transformation would be made

Table 4. Crystallographic data obtained directly from spot patterns of crystals belonging to the six crystal systems.

<u>Crystal System</u>	<u>Plane of Orientation</u>	<u>Crystallographic data</u>
Cubic	(100)	\underline{d}_{100}
Tetragonal	(100)	$\underline{d}_{100}, \underline{d}_{001}$
Tetragonal	(001)	\underline{d}_{100}
Orthorhombic	(100)	$\underline{d}_{010}, \underline{d}_{001}$
Orthorhombic	(010)	$\underline{d}_{100}, \underline{d}_{001}$
Orthorhombic	(001)	$\underline{d}_{100}, \underline{d}_{010}$
Hexagonal	(001)	\underline{d}_{100}
Monoclinic	(100)	$\underline{d}_{010}, (\underline{d}_{001})_p, [(\underline{d}_{001})_p = \underline{c}]$
Monoclinic	(010)	$\underline{d}_{100}, \underline{d}_{001}, \beta$
Monoclinic	(001)	$(\underline{d}_{100})_p, \underline{d}_{010}, [(\underline{d}_{100})_p = \underline{a}]$
Triclinic	(100)	$(\underline{d}_{010})_p, (\underline{d}_{001})_p, \alpha, [(\underline{d}_{010})_p / \sin \alpha = \underline{b}], [(\underline{d}_{001})_p / \sin \alpha = \underline{c}]$
Triclinic	(010)	$(\underline{d}_{100})_p, (\underline{d}_{001})_p, \beta, [(\underline{d}_{100})_p / \sin \beta = \underline{a}], [(\underline{d}_{001})_p / \sin \beta = \underline{c}]$
Triclinic	(001)	$(\underline{d}_{100})_p, (\underline{d}_{010})_p, \gamma, [(\underline{d}_{100})_p / \sin \gamma = \underline{a}], [(\underline{d}_{010})_p / \sin \gamma = \underline{b}]$

to give the proper unit cell. The spot patterns obtained from triclinic crystals represent projections of the $hk0$, $h0l$, or $0kl$ reciprocal nets upon the plane of orientation.

Commonly only those crystals that have perfect cleavage or which crystallize as thin plates or tablets of constant thickness give single-crystal patterns suitable for measurement. Although spot patterns can be obtained from crystals that vary in thickness, the patterns are usually so distorted that they cannot be measured with any accuracy.

The main sources of error in evaluation of cell parameters from EDU single-crystal patterns arise from: 1) limitations in the precision of measurement, and 2) deviation of the crystal face from the horizontal. The precision of measurement is governed by the shape, size, and intensity of the spots and varies according to the particular substance under examination. The deviation of a crystal from the ideal orientation can introduce very large errors if care is not taken to orient the crystal so that one face is approximately normal to the beam. For small deviations (within 5°), the error introduced into the spot pattern will be only a few parts per thousand.

The peculiarities of the electron-diffraction technique must be taken into account in the interpretation of electron-diffraction powder patterns. Consider an aggregate of crystals which are small thin plates or flakes oriented with the basal pinacoid parallel to the substrate of the specimen mount but with all possible orientations in the plane of the substrate. The electron-diffraction powder pattern obtained from these crystals will show a number of evenly blackened rings. Measurement of these rings will yield for the most part the projected quantities $\left| \frac{H}{hkl} \right|_p$ of one net, i.e., the same data given by the spot

pattern of one crystal of the aggregate. The projected quantities $|\frac{H}{\lambda} \sin \theta|_p$ are obtained from the oriented powder pattern because the reciprocal lattice points of each crystal in the aggregate are extended into rods. If an electron-diffraction powder pattern were obtained from an aggregate of small, equidimensional, randomly oriented crystals where there is no extension of reciprocal lattice points into rods, measurement of the rings would yield the quantities $|\frac{H}{\lambda} \sin \theta|$, i.e., the same quantities that are given by an X-ray diffraction powder pattern. In Part II of this paper a method of indexing oriented electron-diffraction powder patterns is given.

REFERENCES

- Buckley, H. E., 1951, Crystal growth: New York, John Wiley & Sons, Inc.
- Christ, C. L., 1953, Studies of borate minerals: I. X-ray crystallography of colemanite: Am. Mineralogist, v. 38, p. 411-415.
- Drumond, D. G., 1950, The practice of electron microscopy: Royal Microsc. Soc. Jour., v. 70, p. 1-158.
- Hall, C. E., 1953, Introduction to electron microscopy: New York, McGraw-Hill Book Co.
- James, R. W., 1954, The optical principles of the diffraction of X-rays: London, G. Bell and Sons, Ltd.
- Picard, R. G., and Reisner, J. H., 1946, Universal electron microscope as a high resolution diffraction camera: Rev. Sci. Instruments, v. 17, p. 484-489.
- Ross, Malcolm, 1958, Mineralogical applications of electron diffraction: II. Results of studies of some vanadium minerals of the Colorado Plateau: Am. Mineralogist.
- Swanson, H. E., and Tatge, E., 1953, Standard X-ray diffraction powder patterns: Natl. Bur. Standards Circ. 539, v. 1.
- Zachariasen, W. H., 1929, The crystal structure of $KClO_3$: Zeitschr. für Kristallographie, v. 71, p. 501-516.